

## H<sub>2</sub> Ortho–Para Spin Conversion on Inhomogeneous Grain Surfaces. II. impact of the rotational energy difference between adsorbed ortho-H<sub>2</sub> and para-H<sub>2</sub> and implication to deuterium fractionation chemistry

KENJI FURUYA,<sup>1</sup> TOSHIKI SUGIMOTO,<sup>2</sup> KAZUNARI IWASAKI,<sup>3,4</sup> MASASHI TSUGE,<sup>5</sup> AND NAOKI WATANABE<sup>5</sup>

<sup>1</sup>RIKEN Pioneering Research Institute, 2-1 Hirosawa, Wako-shi, Saitama 351-0198, Japan

<sup>2</sup>Department of Materials Molecular Science, Institute for Molecular Science, Myodaiji, Okazaki, Aichi 444-8585, Japan

<sup>3</sup>Center for Computational Astrophysics/Division of Science, National Astronomical Observatory of Japan, Mitaka, Tokyo 181-8588, Japan

<sup>4</sup>Astronomical Science Program, The Graduate University for Advanced Studies (SOKENDAI), 2-21-1 Osawa, Mitaka, Tokyo 181-8588, Japan

<sup>5</sup>Institute of Low Temperature Science, Hokkaido University, Sapporo, Hokkaido 060-0819, Japan

(Received; Revised; Accepted)

Submitted to ApJ

### ABSTRACT

We investigate how the H<sub>2</sub> ortho-to-para ratio (OPR) and deuterium fractionation in star-forming regions are affected by nuclear spin conversion (NSC) on dust grains. Particular focus is placed on the rotational energy difference between ortho-H<sub>2</sub> (o-H<sub>2</sub>) and para-H<sub>2</sub> (p-H<sub>2</sub>) on grain surfaces. While the ground state of o-H<sub>2</sub> has a higher rotational energy than that of p-H<sub>2</sub> by 170.5 K in the gas phase, this energy difference is expected to become smaller on solid surfaces, where interactions between the surface and adsorbed H<sub>2</sub> molecules affect their rotational motion. A previous study by Furuya et al. (2019) developed a rigorous formulation of the rate for the temporal variation of the H<sub>2</sub> OPR via the NSC on grains, assuming that adsorbed o-H<sub>2</sub> has higher rotational energy than adsorbed p-H<sub>2</sub> by 170.5 K, as in the gas phase. In this work, we relax the assumption and re-evaluate the rate, varying the rotational energy difference between their ground states. The re-evaluated rate is incorporated into a gas-ice astrochemical model to study the evolution of the H<sub>2</sub> OPR and the deuterium fractionation in prestellar cores and the outer, cold regions of protostellar envelopes. The inclusion of the NSC on grains reduces the timescale of the H<sub>2</sub> OPR evolution and thus the deuterium fractionation, at densities of  $\gtrsim 10^4$  cm<sup>-3</sup> and temperatures of  $\lesssim 14$ –16 K (depending on the rotational energy difference), when the ionization rate of H<sub>2</sub> is  $10^{-17}$  s<sup>-1</sup>.

*Keywords:* astrochemistry — ISM: molecules

### 1. INTRODUCTION

The deuterium fractionation ratio of molecules in star- and planet-forming regions is a useful tool to investigate where and how the molecules were formed, and to investigate the possible chemical link between the interstellar molecules and the primitive materials in the solar system (e.g., Ceccarelli et al. 2014; Nomura et al. 2023). Elemental chemical processes relevant to the deuterium fractionation in the gas phase and on the solid surface have been extensively studied by laboratory experiments and quantum chemical calculations (e.g., Watson 1976; Nagaoka et al. 2005; Hidaka et al. 2009; Ratajczak et al. 2009; Roueff et al. 2013; Cooper & Kästner 2019; Hillenbrand et al. 2019; Jiménez-Redondo et al. 2024). It is well established that the starting point of the deuterium fractionation is the isotope exchange reaction,



At a typical temperature of molecular clouds,  $\sim 10$  K, the backward reaction is inefficient due to the endothermicity (but see below) and thus  $\text{H}_2\text{D}^+$  becomes abundant with time with respect to  $\text{H}_3^+$ . Since  $\text{H}_3^+$  plays a central role in the interstellar chemistry, the deuterium enrichment in  $\text{H}_3^+$  is transferred to other gaseous and icy molecules (e.g., Tielens 1983; Brown & Millar 1989). As a result, all molecules except for  $\text{H}_2$  are expected to have a higher D/H ratio than the elemental deuterium-to-hydrogen ratio of  $1.5 \times 10^{-5}$  (Linsky 2003). Indeed, observations have found orders of magnitude enhancement in the D/H ratio of various molecules not only in molecular clouds but also in protostellar sources and protoplanetary disks (see Ceccarelli et al. 2014; Nomura et al. 2023, for recent reviews).

$\text{H}_2$  and  $\text{H}_3^+$  have two nuclear spin configurations, ortho and para; the nuclear-spin wave functions of ortho and para states are symmetric and antisymmetric, respectively, with respect to the permutations of the nuclei. The endothermicity of the isotope exchange reaction (1) in the reverse direction ( $\Delta E$ ) depends on the nuclear spin state of  $\text{H}_2$  and that of  $\text{H}_3^+$  isotopologues. Thus, their ortho-to-para ratios (OPRs) are the critical parameters for the overall deuterium fractionation chemistry (e.g., Pagani et al. 1992; Flower et al. 2006). The OPRs of  $\text{H}_3^+$  and  $\text{H}_2\text{D}^+$  are mostly determined by the proton exchange with  $\text{H}_2$ , and given as functions of the  $\text{H}_2$  OPR and the gas temperature ( $T_g$ ) (Gerlich et al. 2002). Thus, the  $\text{H}_2$  OPR is of primary importance. Figure 1 shows the steady-state  $\text{H}_2\text{D}^+/\text{H}_3^+$  abundance ratio as a function of  $T_g$ , varying in the  $\text{H}_2$  OPR. When the  $\text{H}_2$  OPR is greater than  $\sim 10^{-3}$ ,  $\text{H}_2$  rather than CO is the dominant destroyer of  $\text{H}_2\text{D}^+$ , regardless of the CO abundance, and the degrees of the deuterium fractionation depend on the  $\text{H}_2$  OPR (see also Furuya et al. 2015).

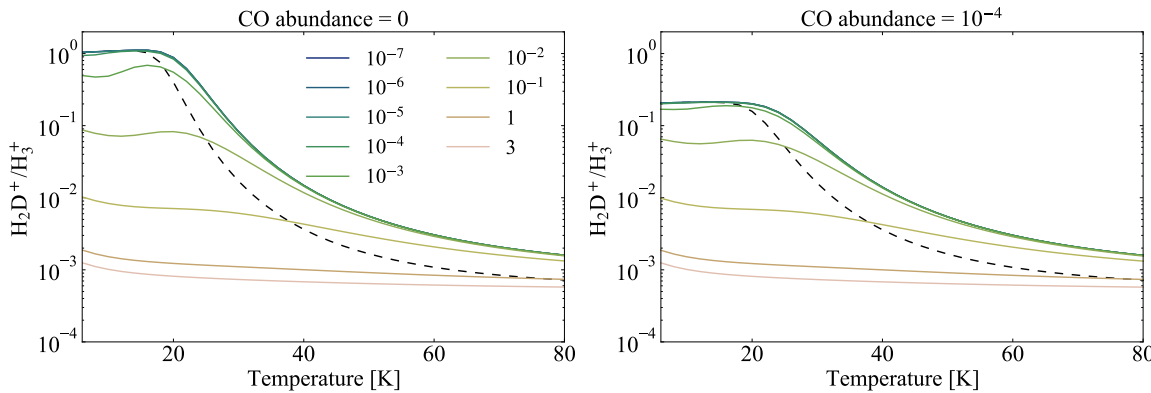


**Figure 1.** The steady-state value of the  $\text{H}_2\text{D}^+/\text{H}_3^+$  abundance ratio as functions of the gas temperature, varying in the  $\text{H}_2$  OPR in the range between  $10^{-7}$  and 3 (solid lines). Dashed lines show the  $\text{H}_2\text{D}^+/\text{H}_3^+$  ratio assuming a thermalized value for the  $\text{H}_2$  OPR. i.e.,  $9 \exp(-170.5/T_g)$ . The gas-phase CO abundance is assumed to be zero in the left panel, while it is assumed to be  $10^{-4}$  in the right panel. These two cases correspond to the minimum and maximum limits of CO abundance, and in reality, the CO abundance would fall between these extremes.

In the ISM, the  $\text{H}_2$  OPR is determined by the competition among the three processes: the  $\text{H}_2$  formation via recombination of two H atoms on grain surfaces (Watanabe et al. 2010; Tsuge et al. 2019), the proton exchange reactions between  $\text{H}_2$  and  $\text{H}^+$  (or  $\text{H}_3^+$ ) in the gas phase (Gerlich 1990; Honvau et al. 2011), and the nuclear spin conversion (NSC) on solid surfaces (Ueta et al. 2016; Tsuge et al. 2021a,b). Astrochemical models with deuterium fractionation chemistry often consider the  $\text{H}_2$  formation and the NSC of  $\text{H}_2$  via gas-phase reactions, but commonly neglect the NSC on grain surfaces (e.g., Flower et al. 2006; Sipilä et al. 2013; Taquet et al. 2014; Furuya et al. 2015; Hily-Blant et al. 2018). One exception is Bovino et al. (2017), but they considered the NSC of ortho- $\text{H}_2$  (o- $\text{H}_2$ ) to para- $\text{H}_2$  (p- $\text{H}_2$ ) only, neglecting the conversion in the reverse direction and assuming a single value for  $\text{H}_2$  binding energy. Later Furuya et al. (2019) pointed out the importance of the  $\text{H}_2$  binding energy distribution. They formulated the rates for the temporal evolution of the gas-phase  $\text{H}_2$  OPR via NSC on water ice under the ISM conditions, based on the laboratory-measured NSC conversion timescale and the  $\text{H}_2$  binding energy distribution. In their formulation, the rotational energy difference between the ground state of o- $\text{H}_2$  and p- $\text{H}_2$  was assumed to be the same in the gas phase ( $\Delta E_{\text{op,g}} = 170.5$  K) and on solid surfaces ( $\Delta E_{\text{op,s}}$ ). However, on solid surfaces, the rotational motion of  $\text{H}_2$  molecules is suppressed due to the interaction with the surface and  $\Delta E_{\text{op,s}}$  would be smaller than  $\Delta E_{\text{op,g}}$  (see Section 2.1 and the Appendix for details). In this work, we extend the approach by Furuya et al. (2019) to re-evaluate the rates for the temporal evolution of the  $\text{H}_2$  OPR via NSC on surfaces in the case when  $\Delta E_{\text{op,s}} \leq \Delta E_{\text{op,g}}$ . Moreover, by adding the NSC on surfaces to a gas-ice astrochemical model with deuterium fractionation chemistry (Furuya et al.

2015), we address how the NSC on surfaces affects the deuterium fractionation chemistry in prestellar cores and in protostellar envelopes, treating  $\Delta E_{\text{op,s}}$  as a free parameter.

The rest of this paper is organized as follows. In Section 2, we discuss how the  $\Delta E_{\text{op,s}}$  value affects the evolution of H<sub>2</sub> OPR in the bulk gas under the ISM conditions, and re-evaluate the rates for the temporal evolution of the H<sub>2</sub> OPR via NSC on surfaces under the ISM conditions. The timescale of the H<sub>2</sub> OPR evolution and its steady state value in the ISM are discussed in Section 3. In Section 4, we discuss the impact of the NSC on grain surfaces on the deuterium fractionation in a collapsing prestellar core. In Section 5, we discuss the impact of the NSC on grain surfaces on the H<sub>2</sub> OPR and H<sub>2</sub>D<sup>+</sup> OPR in the outer regions of the protostellar envelope. Our main findings are summarized in Section 6.

## 2. NSC OF H<sub>2</sub> ON GRAIN SURFACES

### 2.1. Rotational energy difference between *ortho* and *para* hydrogen adsorbed on grains

The H<sub>2</sub> OPR in thermal equilibrium is given by

$$\frac{\sum_{J=\text{odd}} \sum_{m=-J}^J d_{I=1} \exp(-E_{J,m}/T)}{\sum_{J=\text{even}} \sum_{m=-J}^J d_{I=0} \exp(-E_{J,m}/T)}, \quad (2)$$

where  $d_{I=1} = 3$  and  $d_{I=0} = 1$  are the nuclear-spin degeneracies and  $T$  is the temperature.  $E_{J,m}$  is the rotational energy of  $(J, m)$  state in Kelvin, where  $J$  is the rotational quantum number, and  $m$  is the quantum number associated with the  $z$ -component of the angular momentum. For gas-phase H<sub>2</sub>, which can rotate freely, the rotational energy does not depend on  $m$ , then Eq. 2 can be rewritten as

$$\frac{\sum_{J=\text{odd}} d_{I=1}(2J+1) \exp(-E_J/T)}{\sum_{J=\text{even}} d_{I=0}(2J+1) \exp(-E_J/T)}, \quad (3)$$

where  $2J+1$  is the rotational degeneracy (e.g., Fukutani & Sugimoto 2013). In the case of three-dimensional free rotation, the rotational energy is given as  $E_J = BJ(J+1)$ , where  $B$  is the rotational constant ( $\sim 7.4$  meV or  $\sim 85$  K for H<sub>2</sub>). Then the rotational energy difference between the lowest rotational level of p-H<sub>2</sub> ( $J = 0$ ) and o-H<sub>2</sub> ( $J = 1$ ) is  $\Delta E_{\text{op,g}} = 2B \sim 170$  K. At the low temperature limit ( $\lesssim 80$  K), where only the ground states of ortho-H<sub>2</sub> (o-H<sub>2</sub>) and para-H<sub>2</sub> (p-H<sub>2</sub>) are relevant and the population of higher rotational states ( $J \geq 2$ ) is negligible, the thermalized value for freely rotating H<sub>2</sub> is approximated by

$$\gamma_g = 9 \exp(-\Delta E_{\text{op,g}}/T_g), \quad (4)$$

where  $T_g$  is the gas temperature. The gas-phase proton exchange reactions tend to change the H<sub>2</sub> OPR closer to  $\gamma_g$  (Gerlich 1990; Le Bourlot 1991). Similarly, the NSC on solid surfaces would change the H<sub>2</sub> OPR closer to the thermalized value on the surfaces, which is discussed below. In Furuya et al. (2019), the thermalized value on the surfaces was assumed to be  $9 \exp(-\Delta E_{\text{op,g}}/T_s)$ , where  $T_s$  is the surface temperature. Throughout this work, we consider only the ground states of o-H<sub>2</sub> ( $J = 1$ ) and p-H<sub>2</sub> ( $J = 0$ ), unless otherwise stated.

In proximity to surfaces, the surface-molecule interaction influences the rotational motion, and the rotational symmetry is broken in general. Whereas heavy molecules stop rotating on surfaces with the molecular axis fixed to the surface, the lightest molecule like H<sub>2</sub> retains its rotational motion even under the anisotropic surface potential due to the quantum effect (Fukutani & Sugimoto 2013). Under the anisotropic surface potential, the degeneracy of the  $J = 1$  state is lifted and  $(J, m) = (1, 0)$  and  $(1, \pm 1)$  states are shifted, while the  $J = 0$  state shows no shift (Figure 2 and see Appendix for more details). Which of the  $(1, 0)$  or  $(1, \pm 1)$  states becomes the lowest in energy for o-H<sub>2</sub> depends on the property of anisotropic surface potential. Throughout this work, we assume that  $(1, \pm 1)$  states, which correspond to the case of a two-dimensional hindered rotor, are the ground states of adsorbed o-H<sub>2</sub>; i.e., the  $V_2 > 0$  case given in Fig. 2. In addition, we neglect the  $(1, 0)$  state for simplicity, because at the low temperatures ( $\lesssim 20$  K), most o-H<sub>2</sub> is expected to occupy the ground  $(1, \pm 1)$  state.

Under these assumptions, we express the thermalized value of OPR for adsorbed  $\text{H}_2$  as

$$\gamma_s = 6 \exp(-\Delta E_{\text{op},s}/T_s), \quad (5)$$

where  $\Delta E_{\text{op},s}$  corresponds to the energy difference between  $(J, m) = (0, 0)$  and  $(1, \pm 1)$  states on surfaces. If we choose  $(J, m) = (1, 0)$  as the ground state of adsorbed o- $\text{H}_2$ , the pre-exponential factor becomes three. The value of  $\Delta E_{\text{op},s}$  is much more important for  $\gamma_s$  than that of the pre-exponential factor.

Although the actual value of  $\Delta E_{\text{op},s}$  is unknown, the allowed values of  $\Delta E_{\text{op},s}$  can be constrained to some extent. Under the surface potential with extremely large rotational anisotropy, the rotational motion tends to be restricted to the surface-parallel direction. The rotational energy for two-dimensional hindered rotation is given as  $BJ^2$ . Then the rotational energy difference between the ground state of p- $\text{H}_2$  and o- $\text{H}_2$  becomes  $\Delta E_{\text{op},2\text{Drot}} = B \sim 85$  K, which is about a half of  $\Delta E_{\text{op},g}$ . In reality, where the surface potential does not have extremely large rotational anisotropy,  $\Delta E_{\text{op},s}$  would be somewhere between  $\Delta E_{\text{op},g}$  and  $\Delta E_{\text{op},2\text{Drot}}$  ( $\Delta E_{\text{op},2\text{Drot}} \leq \Delta E_{\text{op},s} \leq \Delta E_{\text{op},g}$ ; see Appendix for more detail). For example, assuming  $\Delta E_{\text{op},s} = \Delta E_{\text{op},2\text{Drot}}$  and  $T_g = T_s = 10$  K,  $\gamma_s$  is  $1 \times 10^{-3}$ , which is much larger than  $\gamma_g$  at 10 K ( $4 \times 10^{-7}$ ).

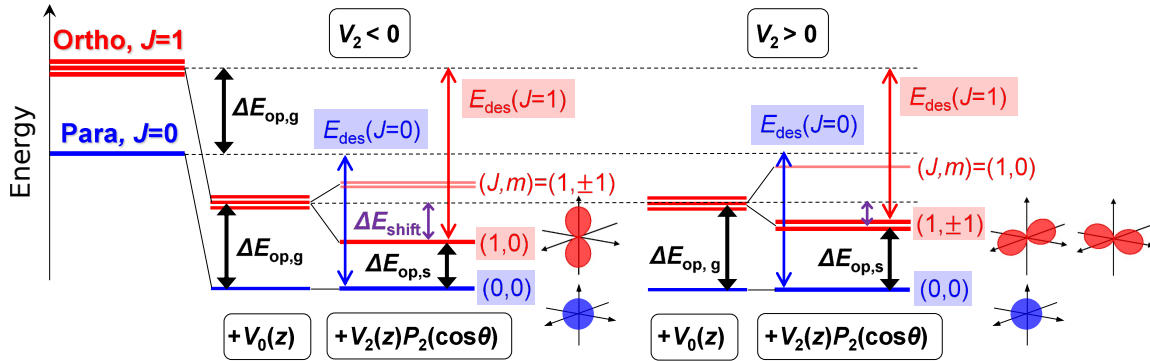


**Figure 2.** Energy level diagram for p- $\text{H}_2$  ( $J = 0$ ) and o- $\text{H}_2$  ( $J = 1$ ) rotational states in the gas phase and on solid surfaces when the surface potential is given by  $V(z, \theta) = V_0(z) + V_2 P_2(\cos \theta)$ , where  $P_2(\cos \theta)$  is the second order Legendre polynomial, and  $V_0(z)$  and  $V_2$  are the isotropic surface potential and the degree of anisotropy, respectively. The number of lines in each level means the rotational degeneracy. Schematic illustrations show the probability distribution of the molecular axis for the respective states,  $|Y_{0,0}|^2$ ,  $|Y_{1,0}|^2$ ,  $|Y_{1,1}|^2$ , and  $|Y_{1,-1}|^2$ , where  $Y_{J,m}$  is the spherical harmonics. See Appendix for more details.

## 2.2. Binding energy difference between ortho and para hydrogen

As most  $\text{H}_2$  is present in the gas phase in the ISM rather than on grains, the exchange of gaseous and icy  $\text{H}_2$  is the rate-limiting step for the temporal evolution of the gas-phase  $\text{H}_2$  OPR via the NSC on grain surfaces (Furuya et al. 2019). In addition, the efficiency of nuclear spin state conversion for an adsorbed  $\text{H}_2$  molecule prior to desorption depends on its residence time on the surface. Then, alongside  $\Delta E_{\text{op},s}$ , another important parameter would be the binding energy difference between o- $\text{H}_2$  and p- $\text{H}_2$ . As o- $\text{H}_2$  is sensitive to the anisotropic part of the surface potential, while p- $\text{H}_2$  is not, o- $\text{H}_2$  has a higher binding energy than p- $\text{H}_2$  by  $\Delta E_{\text{op},g} - \Delta E_{\text{op},s}$  (Fukutani & Sugimoto 2013, see Fig. 2). Then, the  $\text{H}_2$  OPR on the surface may not be directly reflected in the gas phase after thermal desorption, because of the smaller desorption rate of o- $\text{H}_2$  than p- $\text{H}_2$ . Actually, in the case when a single binding energy characterizes a surface, the two effects ( $\Delta E_{\text{op},s} \leq \Delta E_{\text{op},g}$  and higher binding energy of o- $\text{H}_2$  than p- $\text{H}_2$ ) are canceled out;  $\gamma_s \times \exp(-(\Delta E_{\text{op},g} - \Delta E_{\text{op},s})/T_s) \approx \gamma_g$ . In reality, however, surfaces contain various binding sites with different potential energy depths, and  $\text{H}_2$  can hop between different sites by thermal hopping. Then, it is not obvious how the value of  $\Delta E_{\text{op},s}$  affects  $\text{H}_2$  OPR in the gas phase after thermal desorption under the ISM conditions.

## 2.3. Numerical model

Here we explore how the value of  $\Delta E_{\text{op},s}$  affects the temporal evolution of the  $\text{H}_2$  OPR under the ISM conditions. In the case where  $\Delta E_{\text{op},s} = \Delta E_{\text{op},g}$ , the conversion rate from o- $\text{H}_2$  to p- $\text{H}_2$  through the adsorption of o- $\text{H}_2$ , subsequent NSC on grains, and the thermal desorption of p- $\text{H}_2$  ( $R_{\text{op},s}$  in a unit of  $\text{cm}^{-3} \text{ s}^{-1}$ ) and the rate of the reverse process,

$R_{\text{po,s}}$ , can be expressed as

$$R_{\text{op,s}} = \eta_{\text{op}} S_{\text{H}_2} (1 - \Theta) R_{\text{col}}(\text{o-H}_2), \quad (6)$$

$$R_{\text{po,s}} = \eta_{\text{po}} S_{\text{H}_2} (1 - \Theta) R_{\text{col}}(\text{p-H}_2), \quad (7)$$

where  $\eta_{\text{op}}$  is the yield of gaseous p-H<sub>2</sub> per o-H<sub>2</sub> adsorption,  $\eta_{\text{po}}$  is the yield of gaseous o-H<sub>2</sub> per p-H<sub>2</sub> adsorption,  $S_{\text{H}_2}$  is the sticking probability of H<sub>2</sub> to the surface,  $\Theta$  is the surface coverage of H<sub>2</sub>, and  $R_{\text{col}}(\text{o-H}_2)$  and  $R_{\text{col}}(\text{p-H}_2)$  are the collisional rates of o-H<sub>2</sub> and p-H<sub>2</sub>, respectively, to grains (Furuya et al. 2019). The factor  $1 - \Theta$  is considered because only one H<sub>2</sub> molecule is assumed to be adsorbed per binding site.  $\eta_{\text{op}}$  (and  $\eta_{\text{po}}$ ) describe the competition between the NSC of H<sub>2</sub> on and the desorption of H<sub>2</sub> from surfaces (Fukutani & Sugimoto 2013; Furuya et al. 2019). The underlying assumption behind the formulation by Furuya et al. (2019) is that H<sub>2</sub> is in the adsorption-desorption equilibrium. As the adsorption and desorption of H<sub>2</sub> reach the equilibrium in a very short timescale ( $\sim 1$  yr ( $10^4 \text{ cm}^{-3}/n(\text{H}_2)$ )), the assumption should be valid in the dense ISM. In addition to Eqs. 6 and 7, the following relation was used in Furuya et al. (2019):

$$\frac{\eta_{\text{op}}}{\eta_{\text{po}}} = 9 \exp\left(-\frac{\Delta E_{\text{op,g}}}{T_s}\right) = \gamma_g. \quad (8)$$

Note that the ratio of  $\eta_{\text{op}}$  to  $\eta_{\text{po}}$  represents the equilibrium H<sub>2</sub> OPR established solely by the NSC on grains. Eqs. 6-8 can be incorporated in any astrochemical models based on the rate-equation approach. One may think that when  $\Delta E_{\text{op,s}} \neq \Delta E_{\text{op,g}}$ , one should simply replace  $\Delta E_{\text{op,g}}$  in Eq. 8 with  $\Delta E_{\text{op,s}}$ . That would be true when a single binding energy for o-H<sub>2</sub> and p-H<sub>2</sub> is considered, and the binding energy of o-H<sub>2</sub> and p-H<sub>2</sub> is the same. However, as mentioned above, it is not obvious when the binding energy has a distribution and o-H<sub>2</sub> is more strongly bound on the surface. This section aims to determine whether the formulation by Furuya et al. (2019) requires any modifications in the case when  $\Delta E_{\text{op,s}} \neq \Delta E_{\text{op,g}}$  and to re-evaluate  $\eta_{\text{op}}$  and  $\eta_{\text{po}}$ .

### 2.3.1. Model setup

Following Furuya et al. (2019), we numerically solve a set of ordinary differential equations for o-H<sub>2</sub> and p-H<sub>2</sub> that include the adsorption of gas-phase H<sub>2</sub>, thermal desorption, thermal hopping, and NSC of adsorbed H<sub>2</sub>, considering various binding sites with different potential energy depths on surfaces:

$$\frac{dn(\text{o-H}_2)}{dt} = -(1 - \Theta(t)) S_{\text{H}_2} R_{\text{col}}(\text{o-H}_2) + n_{\text{gr}} N_{\text{site}} \sum_j [k_{\text{thdes}}(j) \theta_\alpha(j, t) g(j)], \quad (9)$$

$$\begin{aligned} \frac{d\theta_\alpha(i, t)}{dt} = & [1 - \theta(i, t)] S_{\text{H}_2} \frac{\sigma_{\text{gr}}}{N_{\text{site}}} v_{\text{th}} n(\text{o-H}_2) - \sum_j k_{\text{thdes}}(j) \theta_\alpha(j, t) \\ & - \sum_j k_{\text{hop}}(i \rightarrow j) \theta_\alpha(i, t) [1 - \theta(j, t)] g(j) \\ & + [1 - \theta(i, t)] \sum_j [k_{\text{hop}}(j \rightarrow i) \theta_\alpha(j, t) g(j)] \\ & + k_{\beta\alpha}^{\text{surf}} \theta_\beta(i, t) - k_{\alpha\beta}^{\text{surf}} \theta_\alpha(i, t), \end{aligned} \quad (10)$$

where  $\alpha$  and  $\beta$  indicate either ortho ( $o$ ) or para ( $p$ ), and  $n(\text{o-H}_2)$  and  $n(\text{p-H}_2)$  indicate the number density of o-H<sub>2</sub> and p-H<sub>2</sub> in the gas-phase, respectively.  $n_{\text{gr}}$  is the number density of dust grains in a unit gas volume,  $N_{\text{site}}$  is the number of binding sites on a grain surface, and  $k_{\text{thdes}}$  is the rate constant of the thermal desorption. We denote the fraction of binding site  $i$  on the surface as  $g(i)$ , which satisfies

$$\sum_i g(i) = 1. \quad (11)$$

We denote the fraction of binding site  $i$  that are occupied by o-H<sub>2</sub> (p-H<sub>2</sub>) as  $\theta_o(i)$  ( $\theta_p(i)$ ), and  $\theta(i)$  is defined by  $\theta(i) = \theta_o(i) + \theta_p(i)$ . The surface coverage of H<sub>2</sub> at a given time  $t$ ,  $\Theta(t)$ , is defined as

$$\Theta(t) = \sum_i \theta(i, t) g(i). \quad (12)$$

Similarly  $\Theta_\alpha(t)$ , where  $\alpha$  is  $o$  or  $p$ , is defined as

$$\Theta_\alpha(t) = \sum_i \theta_\alpha(i, t) g(i), \quad (13)$$

and thus  $\Theta(t) = \Theta_o(t) + \Theta_p(t)$ .

The first terms in Eqs. 9 and 10 represent adsorption to the surface, where  $\sigma_{\text{gr}}$  is the cross section of a dust grain. The factor  $1 - \Theta$  or  $1 - \theta$  is included, assuming that only one molecule adsorbs per binding site. Then the maximum value of  $\Theta$  is unity, and the formation of  $\text{H}_2$  multilayers does not occur in our models. The second term in Eqs. 9 and 10 represent thermal desorption. The third term in Eq. 10 represents thermal hopping from site  $i$  to site  $j$ , while the fourth term represents the reverse process, where  $k_{\text{hop}}$  is the rate constant of the thermal hopping. The fifth and sixth terms are for ortho-para conversion on surfaces. Initially, all  $\text{H}_2$  are assumed to be present in the gas phase with the OPR( $\text{H}_2$ ) of three (i.e., the statistical value).

The sticking probability of  $\text{H}_2$  is taken from He et al. (2016), which was experimentally measured for a non-porous amorphous solid water (ASW) surface. The experimentally measured sticking probability would be considered as the surface averaged value, while the sticking probability for each site could depend on the energy depth of each site. However, according to the molecular dynamics simulations of the  $\text{H}_2$  sticking on an ASW surface,  $\text{H}_2$  molecules visit several binding sites before remaining bound in one (Molpeceres & Kästner 2020). Then, the use of the surface averaged sticking probability for Eqs. 9 and 10 would be acceptable in this work. As the binding energy distribution of p- $\text{H}_2$ , we adopt the experimentally determined binding energy distribution of  $\text{D}_2$  on non-porous ASW, considering the zero-point energy difference between  $\text{D}_2$  and  $\text{H}_2$  of  $\sim 37$  K (He & Vidali 2014; Amiaud et al. 2015). The binding energy of o- $\text{H}_2$  at each site is set to higher than that of p- $\text{H}_2$  by  $\Delta E_{\text{op,g}} - \Delta E_{\text{op,s}}$  (Section 2.1). The hopping activation energy from site  $i$  to site  $j$  is given by (Cazaux et al. 2017)

$$E_{\text{hop}}(i \rightarrow j) = f \times \min(E_{\text{des}}(i), E_{\text{des}}(j)) + \max(0, E_{\text{des}}(i) - E_{\text{des}}(j)), \quad (14)$$

The hopping-to-binding energy ratio ( $f$ ) for  $\text{H}_2$  is poorly constrained. Laboratory studies found that the value of  $f$  ranges from 0.2 to 0.7, depending on the species on ASW (Kouchi et al. 2021; Furuya et al. 2022). The NSC on grains affects the OPR of overall (gas + ice)  $\text{H}_2$  more efficiently with lowering the hopping activation energy (Furuya et al. 2019). Here we assume a relatively conservative value,  $f = 0.65$ . The NSC timescale of  $\text{H}_2$  ( $\tau_{\text{conv}}^{\text{surf}}$ ) is taken from Ueta et al. (2016), who measured the timescale for ASW by laboratory experiments. From  $\tau_{\text{conv}}^{\text{surf}}$ , the rate constant of the conversion from adsorbed o- $\text{H}_2$  to adsorbed p- $\text{H}_2$  ( $k_{\text{op}}^{\text{surf}}$ ) and that of the reverse process ( $k_{\text{po}}^{\text{surf}}$ ) can be deduced to be (Bron et al. 2016)

$$k_{\text{op}}^{\text{surf}} = 1/(\tau_{\text{conv}}^{\text{surf}}(1 + \gamma_s)), \quad (15)$$

$$k_{\text{po}}^{\text{surf}} = \gamma_s/(\tau_{\text{conv}}^{\text{surf}}(1 + \gamma_s)). \quad (16)$$

Initially, all  $\text{H}_2$  is assumed to be in the gas phase with an OPR of three. We confirmed that the initial value of the  $\text{H}_2$  OPR does not affect our conclusion in this section or the derived values of  $\eta_{\text{op}}$  and  $\eta_{\text{po}}$ . We run a small grid of pseudo-time-dependent models (i.e., the gas density and the temperature are fixed in each model), varying the  $\text{H}_2$  gas density from  $10^3$  to  $10^7 \text{ cm}^{-3}$  and the temperature from 10 to 20 K. Gas and surface temperatures are assumed to be the same. For each pseudo-time-dependent model, we consider the three case where  $\Delta E_{\text{op,s}} = \Delta E_{\text{op,2Drot}}$  (85 K),  $\Delta E_{\text{op,s}} = 120$  K, and  $\Delta E_{\text{op,s}} = \Delta E_{\text{op,g}}$  (170.5 K).

### 2.3.2. Results

Figure 3 shows the temporal evolution of the  $\text{H}_2$  OPR in the gas phase, on the surface, and in desorbing gas from the surface (i.e., the ratio of the thermal desorption rate of o- $\text{H}_2$  to that of p- $\text{H}_2$ ). The dashed lines represent the model with  $\Delta E_{\text{op,s}} = 170.5$  K, while the solid lines represent the model with  $\Delta E_{\text{op,s}} = 85$  K. At 10 K, the evolution of the  $\text{H}_2$  OPR in the gas phase is almost identical regardless of the value of  $\Delta E_{\text{op,s}}$ . The model with  $\Delta E_{\text{op,s}} = 85$  K shows higher  $\text{H}_2$  OPR on the surface compared to the model with  $\Delta E_{\text{op,s}} = 170.5$  K. In contrast, the  $\text{H}_2$  OPR in the desorbing gas is lower in the model with  $\Delta E_{\text{op,s}} = 85$  K than in the model with  $\Delta E_{\text{op,s}} = 170.5$  K, because the binding energy for o- $\text{H}_2$  at a given site is 85 K higher than that for p- $\text{H}_2$ , leading to the lower desorption rate of o- $\text{H}_2$  in the former model. At  $\gtrsim 10^6$  yr, the  $\text{H}_2$  OPR of desorbing gas and in the gas phase become  $\sim 6 \exp(-170.5/T)$  in both two models rather than  $\gamma_s = 6 \exp(\Delta E_{\text{op,s}}/T)$  or  $\gamma_g = 9 \exp(\Delta E_{\text{op,g}}/T)$ .

At  $\gtrsim 14$  K, unlike at 10 K, the temporal evolution of the  $\text{H}_2$  OPR in the gas phase depends on the value of  $\Delta E_{\text{op,s}}$ ; the timescale of the decrease of the  $\text{H}_2$  OPR is shorter in the model with  $\Delta E_{\text{op,s}} = 85$  K than in the model with  $\Delta E_{\text{op,s}} = 170.5$  K. This is because the higher binding energy of o- $\text{H}_2$  in the model with  $\Delta E_{\text{op,s}} = 85$  K results in

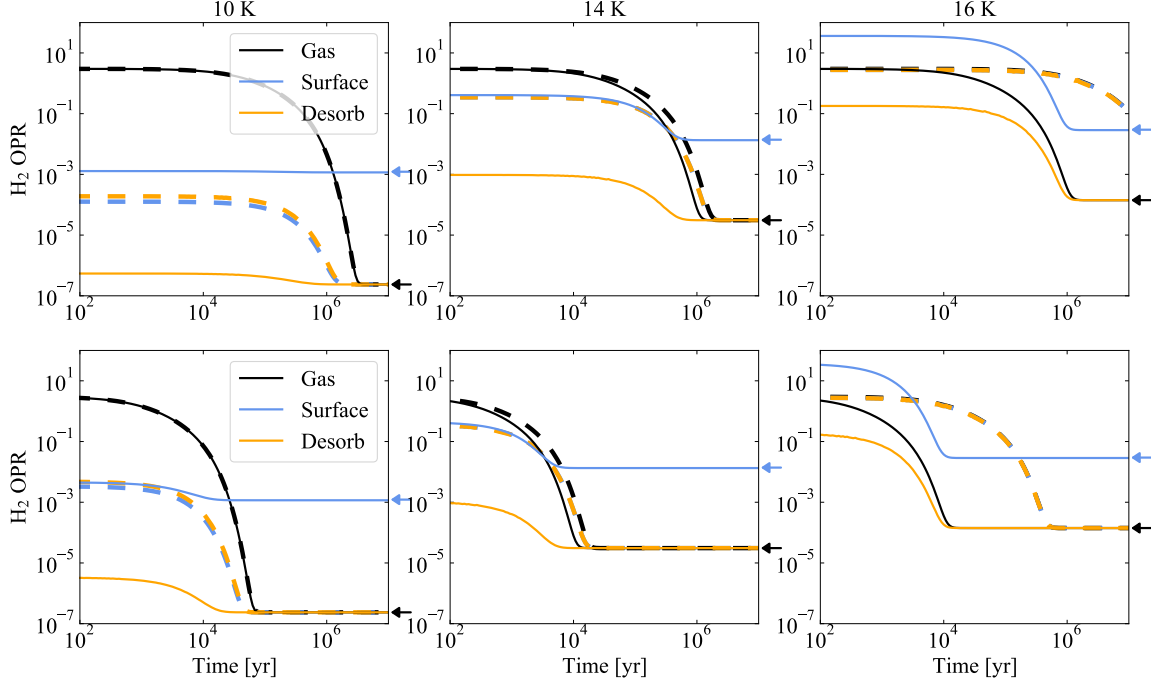


**Figure 3.** Temporal evolution of the H<sub>2</sub> OPR in the gas phase, on the surface, and in desorbing gas from the surface. Dashed lines show the model with  $\Delta E_{\text{op,s}} = 170.5$  K, while solid lines show the model with  $\Delta E_{\text{op,s}} = 85$  K. The H<sub>2</sub> gas density is  $10^4$  cm<sup>-3</sup> in top panels, while it is  $10^6$  cm<sup>-3</sup> in lower panels. The temperature is from 10 K, 14 K, and 16 K in the left, middle, and right panels, respectively. Note that in the model with  $\Delta E_{\text{op,s}} = 170.5$  K, the OPRs on the surface and in the desorbing gas are similar, and the lines for them are partially overlapping in the figure. Arrows on the right margin indicate  $6 \exp(-170.5/T)$  (black) and  $\gamma_s$  (blue).

longer residence time on the surface, which in turn leads to more efficient NSC than in the model with  $\Delta E_{\text{op,s}} = 170.5$  K. On the other hand, the steady-state value of the H<sub>2</sub> OPR in the gas phase does not depend on  $\Delta E_{\text{op,s}}$  and is given by  $6 \exp(-170.5/T)$  as in the case of the temperature of 10 K. We confirmed that this conclusion holds even when  $\Delta E_{\text{op,s}}$  depends on sites by running additional models in which  $\Delta E_{\text{op,s}}$  for a site with the binding energy of  $E_{\text{des}}$  is given by  $\Delta E_{\text{op,2Drot}} \times (E_{\text{des}}/E_{\text{des,max}})$ , where  $E_{\text{des,max}}$  is the maximum binding energy. These results indicate that when  $\Delta E_{\text{op,s}} \neq \Delta E_{\text{op,g}}$ , instead of Eq. 8, the slightly modified one should be used:

$$\frac{\eta_{\text{op}}}{\eta_{\text{po}}} = 6 \exp\left(-\frac{\Delta E_{\text{op,g}}}{T_s}\right). \quad (17)$$

Under the adsorption-desorption equilibrium which is established within  $\sim 1$  yr ( $10^4$  cm<sup>-3</sup>/n(H<sub>2</sub>)), the parameter  $\eta_{\text{op}}$  is derived from the desorption rates of o-H<sub>2</sub> and p-H<sub>2</sub> in the numerical simulations (see Sec. 3.4 of Tsuge et al. 2021a). The resulting  $\eta_{\text{op}}$  at the density of  $10^4$  cm<sup>-3</sup> is shown in Figure 4. Note that although  $\Delta E_{\text{op,s}}$  does not explicitly included in Eqs. 6 and 7,  $\eta_{\text{op}}$  (and  $\eta_{\text{po}}$ ) do depend on the value of  $\Delta E_{\text{op,s}}$ .

Finally, we confirmed that numerically integrating the following equations for the temporal evolution of o-H<sub>2</sub> and p-H<sub>2</sub>, using the derived  $\eta_{\text{op}}$  and  $\eta_{\text{po}}$  (see Eq. 17), successfully reproduces the temporal evolution of the H<sub>2</sub> OPR in the gas phase obtained by solving Eqs. 9 and 10:

$$\frac{dn(\text{o-H}_2)}{dt} = -R_{\text{op,s}} + R_{\text{po,s}}, \quad (18)$$

$$\frac{dn(\text{p-H}_2)}{dt} = -R_{\text{po,s}} + R_{\text{op,s}}. \quad (19)$$

Then, we conclude that in general cases, once  $\eta_{\text{op}}$  is given, the rates for the temporal evolution of the H<sub>2</sub> OPR through NSC on surfaces are given by Eqs. 6, 7 and 17, which can be included in any astrochemical models based on the rate-equation approach.

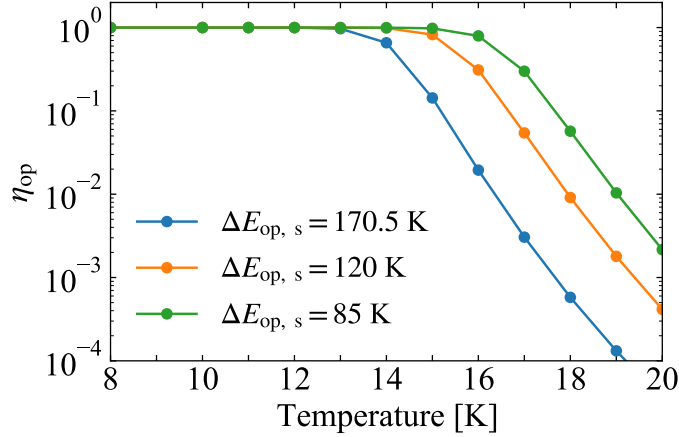


**Figure 4.** The parameter  $\eta_{\text{op}}$  as functions of the temperature in the case when  $\Delta E_{\text{op,s}} = 170.5$  K (blue), and  $\Delta E_{\text{op,s}} = 120$  K (orange), and  $\Delta E_{\text{op,s}} = 85$  K (green). As the density dependence of  $\eta_{\text{op}}$  is very weak, the values only at the  $\text{H}_2$  density of  $10^4 \text{ cm}^{-3}$  are plotted here.

### 3. TIMESCALE OF THE $\text{H}_2$ OPR EVOLUTION AND ITS STEADY STATE VALUE IN THE ISM

Here we discuss the timescale of the  $\text{H}_2$  OPR evolution and its steady state value ( $\text{OPR}_{\text{st}}$ ) in the ISM, which are determined by the competition among the  $\text{H}_2$  formation, the NSC via the gas-phase reactions, and the NSC on grain surfaces. Assuming all atomic H adsorbed onto dust grains are consumed by the  $\text{H}_2$  formation, the  $\text{H}_2$  formation timescale is given by

$$\tau_{\text{H}_2} = n(\text{H}_2)/(0.5S_{\text{H}_2}R_{\text{col}}(\text{H})), \quad (20)$$

where  $R_{\text{col}}(\text{H})$  is the collisional rate ( $\text{cm}^{-3} \text{ s}^{-1}$ ) of atomic H to dust grains. The NSC timescale via the gas-phase proton exchange reactions is given by

$$\tau_{\text{op,g}} = 1/(k_{\text{op,g}}n(\text{H}_3^+)), \quad (21)$$

$$\tau_{\text{po,g}} = 1/(k_{\text{op,g}}\gamma_g n(\text{H}_3^+)), \quad (22)$$

where  $k_{\text{op,g}}$  is the rate constant of the proton exchange reactions in the gas-phase (Honvaut et al. 2011, 2012; Hily-Blant et al. 2018). Here we consider the proton exchange reactions with  $\text{H}_3^+$  only because the exchange reactions with  $\text{H}_3^+$  are more important than those with  $\text{H}^+$  in the dense ISM (Furuya et al. 2015). We estimate the abundance of  $\text{H}_3^+$  using the analytical method introduced by Aikawa et al. (2015) (see their Sec. 4), but neglecting the presence of  $\text{N}_2\text{H}^+$  and recombination of ions with charged grains. With this method, we can self-consistently estimate the abundance of  $\text{H}_3^+$ ,  $\text{HCO}^+$ , and electrons for given parameters, including the cosmic-ray ionization rate of  $\text{H}_2$  ( $\zeta$ ), the CO abundance, temperature, and the gas density. Finally, the timescale for the NSC on surfaces is given by

$$\tau_{\text{op,s}} = n(\text{o-H}_2)/(\eta_{\text{op}}S_{\text{H}_2}(1 - \Theta)R_{\text{col}}(\text{o-H}_2)), \quad (23)$$

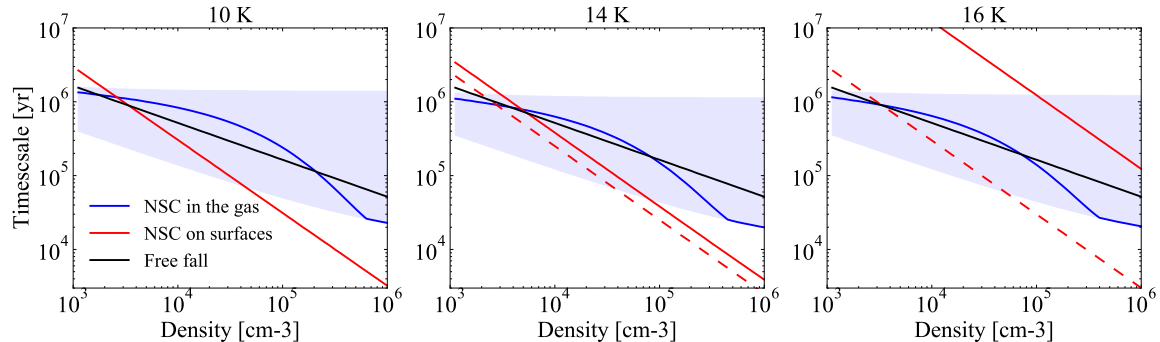
$$\tau_{\text{po,s}} = n(\text{p-H}_2)/(\eta_{\text{po}}S_{\text{H}_2}(1 - \Theta)R_{\text{col}}(\text{p-H}_2)). \quad (24)$$

Figure 5 shows  $\tau_{\text{op,g}}$ ,  $\tau_{\text{op,s}}$ , and the free-fall timescale ( $\tau_{\text{ff}}$ ) the last of which is a measure of the dynamical timescale of star formation, representing the shortest possible timescale for gravitational collapse. In the figure, it is assumed that the cosmic-ray ionization rate of  $\text{H}_2$  is  $10^{-17} \text{ s}^{-1}$ , the dust-to-gas mass ratio is 0.01, and the dust grain radius is  $0.1 \mu\text{m}$ . It is worth noting the different density dependence of the timescales. Since  $R_{\text{col}}(\text{H}) \propto n_{\text{gr}}n(\text{H})$ , and since  $n(\text{H}) \sim 1/(\zeta/10^{-17} \text{ s}^{-1}) \text{ cm}^{-3}$ , regardless of the gas density, in regions where the UV radiation is well-shielded and hydrogen is mostly locked up in  $\text{H}_2$  (e.g., Goldsmith & Li 2005),  $\tau_{\text{H}_2}$  does not depend on the gas density (denoted as  $n_{\text{gas}}$ ), and is  $\sim 3 \times 10^9 \text{ yr}$ , which is much longer than the other timescales (thus not shown in Fig. 5).  $\tau_{\text{op,s}}$  is proportional to  $\sim n_{\text{gas}}^{-1}$ , as the density dependencies of  $\eta$  and  $\Theta$  are relatively weak (Furuya et al. 2019).  $\tau_{\text{op,g}}$  is proportional to  $\sim n_{\text{gas}}^{-0.5}$  when  $\text{H}_3^+$  is the dominant positive charge carrier (i.e., when the CO abundance is low; see the lower end of the blue area in Fig. 5), because the number density of major ions (i.e.,  $\text{H}_3^+$ ) are proportional to  $\sim n_{\text{gas}}^{0.5}$  (e.g., Tielens

2005). When the CO abundance is high (the upper end of the blue area), HCO<sup>+</sup> rather than H<sub>3</sub><sup>+</sup> is the dominant charge carrier and the number density of H<sub>3</sub><sup>+</sup> does not depend on  $n_{\text{gas}}$  (see Eq. 23 of Aikawa et al. 2015), and thus  $\tau_{\text{op},\text{g}}$  neither.  $\tau_{\text{ff}}$  is scaled with  $n_{\text{gas}}^{-0.5}$  (Spitzer 1978). Taken together, the NSC on surfaces has the strongest density dependence, and in regions with the density of  $\gtrsim 10^4 \text{ cm}^{-3}$ , the NSC on surfaces plays a major role in the evolution of the H<sub>2</sub> OPR. The latter argument is consistent with the hydrodynamical simulations of collapsing filaments coupled with chemistry by Lupi et al. (2021), which showed the NSC in the gas-phase is more important than that on grains in the filaments where the gas density is mostly  $\lesssim 10^4 \text{ cm}^{-3}$ .

The H<sub>2</sub> OPR would reach the steady state at a density higher than  $10^5 \text{ cm}^{-3}$ , as the timescale of NSC is much shorter than the free-fall timescale. If the dynamical evolution proceeds more slowly than the free-fall timescale due to support from thermal pressure, magnetic fields, or other effects, this threshold density ( $10^5 \text{ cm}^{-3}$ ) becomes lower. While  $\tau_{\text{op},\text{g}}$  and  $\tau_{\text{ff}}$  do not strongly depend on the temperature,  $\tau_{\text{op},\text{s}}$  becomes larger with increasing the temperature. When  $\Delta E_{\text{op},\text{s}} = 170.5 \text{ K}$ , the NSC on grains is negligible compared to the NSC in the gas phase at  $\gtrsim 16 \text{ K}$ . On the other hand, when  $\Delta E_{\text{op},\text{s}} = 85 \text{ K}$ , even at 16 K, the NSC on grains is more efficient than that in the gas phase. At 20 K, the NSC on grains becomes negligible compared to the NSC in the gas phase even when  $\Delta E_{\text{op},\text{s}} = 85 \text{ K}$ . Then, the actual value of  $\Delta E_{\text{op},\text{s}}$  becomes critical at slightly warmer temperatures than the typical temperature of molecular clouds ( $\sim 10 \text{ K}$ ).

Note that in this section, we fixed the cosmic ionization rate of H<sub>2</sub> to be  $\zeta = 10^{-17} \text{ s}^{-1}$ . As the abundances of ion species increases with increasing  $\zeta$ , the timescale for the NSC in the gas phase becomes shorter with increasing  $\zeta$ . For the galactic center environments, where  $\zeta$  is  $10^{-14} \text{ s}^{-1}$  or even higher (Le Petit et al. 2016), the threshold density at which NSC on grains is more efficient than that in the gas phase would increase to above  $\sim 10^5\text{-}10^6 \text{ cm}^{-3}$ . In addition, the timescale of the NSC in the gas phase is sufficiently short compared to the free-fall timescale. Then, in that environment, the role of NSC on grains would be minor.



**Figure 5.** Conversion timescale of o-H<sub>2</sub> to p-H<sub>2</sub> via the NSC on grain surfaces when  $\Delta E_{\text{op},\text{s}} = 170.5 \text{ K}$  (red solid lines) and when  $\Delta E_{\text{op},\text{s}} = 85 \text{ K}$  (red dashed lines) as functions of the gas density. Black solid line indicates the free-fall timescale ( $\tau_{\text{ff}}$ ). The blue area indicates the conversion timescale of o-H<sub>2</sub> to p-H<sub>2</sub> via the gas-phase proton exchange reaction with the upper and lower ends corresponding to the CO abundance of  $10^{-4}$  and  $10^{-6}$ , respectively. The blue solid line indicates the case when the CO abundance is given by  $10^{-4} \exp(-\tau_{\text{ff}}/\tau_{\text{freeze}})$ , where  $\tau_{\text{freeze}}$  is the freeze-out timescale of CO onto dust grains, with the minimum CO abundance of  $10^{-6}$ . Gas and dust temperatures are the same and assumed to be 10 K, 14 K, and 16 K in the left, middle, and right panels, respectively.

In the case where only the H<sub>2</sub> formation and the proton exchange reactions in the gas phase are considered, the analytical expression of OPR<sub>st</sub> was derived by Furuya et al. (2015) (see their Appendix A). It is straightforward to include the contribution of the NSC on solid surfaces, and one can obtain

$$\text{OPR}_{\text{st}} = \frac{\tau_{\text{op}}/\tau_{\text{po}} + b_0 \tau_{\text{op}}/\tau_{\text{H}_2}}{1 + (1 - b_0) \tau_{\text{op}}/\tau_{\text{H}_2}}, \quad (25)$$

where  $b_0$  is the branching ratio to form o-H<sub>2</sub> upon the H<sub>2</sub> formation (0.75; Watanabe et al. 2010). The conversion timescale of o-H<sub>2</sub> to p-H<sub>2</sub> ( $\tau_{\text{op}}$ ) is defined as

$$\frac{1}{\tau_{\text{op}}} = \frac{1}{\tau_{\text{op},\text{g}}} + \frac{1}{\tau_{\text{op},\text{s}}}. \quad (26)$$

The NSC timescale of p-H<sub>2</sub> to o-H<sub>2</sub> ( $\tau_{po}$ ) is defined in a similar way. Although  $\tau_{H_2}$  is much larger than the NSC timescales, the former is still relevant to the steady state value of H<sub>2</sub> OPR. This is because the statistical value of three is much larger than  $\gamma_g$  at low temperatures ( $\sim 10$  K). Figure 6 shows the steady state value of H<sub>2</sub> OPR predicted by Eq. 25 varying gas density and temperature. The steady-state H<sub>2</sub> OPR becomes lower than that without the NSC on grain surfaces, in particular at the temperature of 10 K and the density of  $> 10^4$  cm<sup>-3</sup>. The difference due to the NSC on grains would be minor for deuterium fractionation chemistry, because the steady state H<sub>2</sub> OPR is lower than  $10^{-3}$  even in the case without the NSC on grains (see Fig. 1). Thus, the primary role of NSC on grains is to shorten the H<sub>2</sub> OPR timescale at the density of  $> 10^4$  cm<sup>-3</sup> and the temperature of  $\lesssim 14$ –16 K (depending on the value of  $\Delta E_{op,s}$ ), rather than to lower the steady-state value of the H<sub>2</sub> OPR.

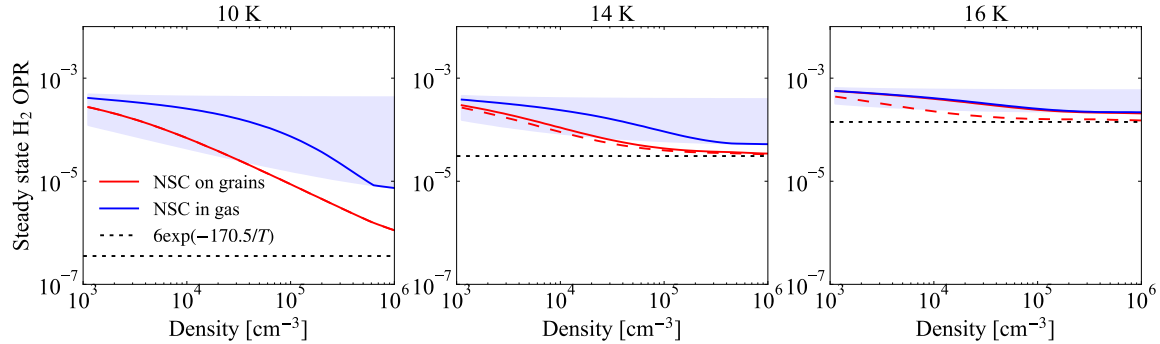


**Figure 6.** A steady state value of H<sub>2</sub> OPR as a function of gas density. Gas and dust temperatures are the same and assumed to be 10 K, 14 K, and 16 K in the left, middle, and right panels, respectively. Red solid lines indicate the case when both the NSC on grains and that in the gas phase are included. The blue area indicates the case when only the NSC in the gas-phase is considered, with the upper and lower ends corresponding to the CO abundance of  $10^{-4}$  and  $10^{-6}$ , respectively. The blue solid line indicates the case when the CO abundance is given by  $10^{-4} \exp(-\tau_{ff}/\tau_{freeze})$ , where  $\tau_{freeze}$  is the freeze-out timescale of CO onto dust grains, with the minimum CO abundance of  $10^{-6}$ . Black dotted lines correspond to  $6 \exp(-170.5/T)$ .

#### 4. MODELING OF DEUTERIUM FRACTIONATION CHEMISTRY WITH THE H<sub>2</sub> OPR IN PRESTELLAR CORES

##### 4.1. Astrochemical model description

Here we discuss the impact of the NSC on grain surfaces on the deuterium fractionation in a collapsing prestellar core. To this end, we use a gas-ice astrochemical code, Rokko, presented in Furuya et al. (2015), which considers mono-, doubly, and triply deuterated species and nuclear spin states of H<sub>2</sub>, H<sub>3</sub><sup>+</sup>, and their isotopologues. We adopt the three-phase model, which includes chemical species in the gas phase, on the surface of the ice, and in the bulk ice mantle, assuming that the bulk mantle has uniform chemical composition (Hasegawa & Herbst 1993). We consider gas-phase reactions, interactions between gas and (icy) grain surfaces, and surface reactions as chemical processes. As non-thermal desorption mechanisms, which are more important than thermal desorption at low temperatures ( $\sim 10$  K), photodesorption, chemical desorption, and whole grain heating by cosmic rays are taken into account. See Furuya et al. (2015) and references therein for more details.

There are some updates from Furuya et al. (2015). We use the species-to-species rate coefficients for the H<sub>2</sub>–H<sub>3</sub><sup>+</sup> reaction systems from Hily-Blant et al. (2018), assuming local thermodynamic equilibrium for the rotationally excited states within each nuclear spin state (see also Sipilä et al. 2017). In Furuya et al. (2015), the rate coefficients for the H<sub>2</sub>–H<sub>3</sub><sup>+</sup> reaction systems were adopted from Hugo et al. (2009), assuming that the species in each nuclear spin state are in their rotational ground states. The rate coefficients for the isotope exchange reactions of D atoms with H<sub>3</sub><sup>+</sup> or H<sub>2</sub>D<sup>+</sup> are set to be  $10^{-12}$  s<sup>-1</sup>, which corresponds to the upper limit value obtained by experiments and quantum chemical calculations (Hillenbrand et al. 2019). In Furuya et al. (2015), their rate coefficients were set to be three orders of magnitude higher ( $10^{-9}$  cm<sup>-3</sup>; Millar et al. 1989) than the values used in this work. As in Furuya et al. (2015), the rate coefficient for the proton exchange reaction of H<sub>2</sub> with H<sup>+</sup> is taken from Honvault et al. (2011, 2012), and the OPR upon the H<sub>2</sub> formation is set to the nuclear-spin statistical value of 3 (Watanabe et al. 2010; Tsuge et al. 2019). The NSC of H<sub>2</sub> on surfaces is newly considered with Eqs. 6, 7, and 17. The parameter  $\eta$  is taken from the simulation results presented in Section 2.3. We adopt a quasi-steady state treatment of the surface coverage of H<sub>2</sub>,

assuming the adsorption-desorption equilibrium (Furuya 2024). We also adopt the same treatment for HD and D<sub>2</sub> on grain surfaces as H<sub>2</sub>.

The elemental abundances are taken from Aikawa & Herbst (1999). The D/H elemental abundance ratio is set to be  $1.5 \times 10^{-5}$  (Linsky 2003). Initially, hydrogen and deuterium are present as H<sub>2</sub> and HD, respectively. The other elements are initially either neutral atoms or atomic ions, depending on their ionization energy. Astrochemical modeling suggests that the H<sub>2</sub> OPR is much lower than unity in molecular clouds and prestellar cores (Furuya et al. 2015; Lupi et al. 2021). There are some indirect estimates of the H<sub>2</sub> OPR in prestellar cores from the observations of deuterated molecules, suggesting that the H<sub>2</sub> OPR is  $\sim 10^{-2}$  for Barnard 68 (Maret & Bergin 2007) and  $\sim 10^{-2}$  or even higher for L183 (Pagani et al. 2009, 2013). Here the initial H<sub>2</sub> OPR is treated as a free parameter, and three different values ( $10^{-3}$ ,  $10^{-2}$ , and 0.1) are considered.

We simulate the molecular evolution, assuming the physical conditions evolve with time on a timescale of free-fall collapse, mimicking a collapsing prestellar core (Brown & Millar 1989). The initial and final gas densities are set to  $2 \times 10^3$  cm<sup>-3</sup> and  $10^7$  cm<sup>-3</sup>, respectively. The visual extinction ( $A_V$ ) is assumed to increase following  $n_{\text{gas}}^{2/3}$  (Garrod & Pauly 2011) with the initial  $A_V$  of 2 mag. The dust temperature is calculated using Equation (8) in Hocuk et al. (2017) with the floor value of 10 K. The gas temperature is assumed to be the same as the dust temperature. Note that, as the maximum temperature in the physical model is  $\sim 13$  K, the efficiency of the NSC on grains does not depend on  $\Delta E_{\text{op,s}}$  (see Figs. 5 and 6) in this simulation setup. Cosmic-ray ionization rate of H<sub>2</sub> is set to be  $1.3 \times 10^{-17}$  s<sup>-1</sup>.

#### 4.2. Results

Figure 7 shows the abundances of selected species (panels a and b), the H<sub>2</sub> OPR in the gas phase (panels c and d), and the X<sub>2</sub>D<sup>+</sup>/H<sub>3</sub><sup>+</sup> ratio, where X is H or D (e and f), as functions of the gas density in the model with (left panels) and without NSC on grains (right panels). Figure 8 shows ratios of the results obtained without and with NSC on grains for ease of comparison. In our models, the density increases with time on the free-fall timescale, so the horizontal axes can be read as time. In the model without the NSC on grains, the H<sub>2</sub> OPR and the X<sub>2</sub>D<sup>+</sup>/H<sub>3</sub><sup>+</sup> ratios depend on the initial value of the H<sub>2</sub> OPR even at the highest density (or the final simulation time), because  $\tau_{\text{op,g}}$  is larger than  $\tau_{\text{ff}}$  until the CO freeze-out becomes significant (Fig. 5). This trend is qualitatively consistent with the earlier modeling studies (e.g., Flower et al. 2006).

In the case when the NSC on grains is included, the impact of the initial H<sub>2</sub> OPR becomes smaller at the density higher than  $10^4$  cm<sup>-3</sup>, because  $\tau_{\text{op,g}}$  is shorter than  $\tau_{\text{ff}}$  (Fig. 5). Regardless of the initial value, the H<sub>2</sub> OPR becomes as low as  $\sim 10^{-4}$  and the H<sub>2</sub>D<sup>+</sup>/H<sub>3</sub><sup>+</sup> ratio becomes  $>0.1$  at the density of  $\gtrsim 10^5$  cm<sup>-3</sup>. At the highest density ( $\gtrsim 10^6$  cm<sup>-3</sup>), the H<sub>2</sub>D<sup>+</sup>/H<sub>3</sub><sup>+</sup> ratio is around unity and D<sub>3</sub><sup>+</sup> is the most abundant among the H<sub>3</sub><sup>+</sup> isotopologues (e.g., Wakelam et al. 2004). The D<sub>2</sub>H<sup>+</sup>/H<sub>3</sub><sup>+</sup> and D<sub>3</sub><sup>+</sup>/H<sub>3</sub><sup>+</sup> ratios at the highest density also do not depend on the initial H<sub>2</sub> OPR. The X<sub>2</sub>D<sup>+</sup>/H<sub>3</sub><sup>+</sup> ratios in the model with NSC on grains are higher than those in the model without NSC on grains. The impact is more significant for D<sub>2</sub>H<sup>+</sup> and D<sub>3</sub><sup>+</sup> compared to H<sub>2</sub>D<sup>+</sup>, because the H<sub>2</sub>D<sup>+</sup>/H<sub>3</sub><sup>+</sup> ratio saturates around unity due to the H<sub>2</sub>D<sup>+</sup> destruction by HD (i.e., the D<sub>2</sub>H<sup>+</sup> formation). Therefore, including NSC on grains reduces the sensitivity of deuterium fractionation chemistry to the assumed initial H<sub>2</sub> OPR, and enhances the deuterium fractionation at the high densities ( $\gtrsim 10^4$  cm<sup>-3</sup>). It should be noted, however, that the above statement is true for locally formed species, such as ion molecules, but not, e.g., water ice; the icy HDO/H<sub>2</sub>O ratio (dashed lines in the bottom panels) still depends on the initial H<sub>2</sub> OPR at the density higher than  $10^5$  cm<sup>-3</sup> even in the model with the NSC on grains, because water ice continuously forms and accumulates from the beginning to the end of the simulation.

### 5. DISCUSSION

#### 5.1. The OPR of H<sub>2</sub>D<sup>+</sup> in a protostellar envelope

It has been proposed that the H<sub>2</sub> OPR can serve as a chemical clock for star formation, since it is initially 3 upon the H<sub>2</sub> formation, is expected to decrease monotonically over time in cold ( $\sim 10$  K) regions, and the timescale of NSC in the gas phase is long (Section 3). However, as the NSC on grains can shorten the evolutionary timescale of the H<sub>2</sub> OPR, it would be useful to reconsider its usefulness and limitations, particularly at the high-density regions ( $\gtrsim 10^4$  cm<sup>-3</sup>). Deuterium fractionation ratio, such as N<sub>2</sub>D<sup>+</sup>/N<sub>2</sub>H<sup>+</sup>, has often been used as an indirect tracer of the H<sub>2</sub> OPR, because it is difficult to directly observe H<sub>2</sub> in the cold gas ( $\sim 10$  K) (e.g., Pagani et al. 2011). Here we focus on the H<sub>2</sub>D<sup>+</sup> OPR, which has been proposed as the best tracer of the H<sub>2</sub> OPR (Brünken et al. 2014). Since the H<sub>2</sub>D<sup>+</sup> OPR is set by the collision between H<sub>2</sub>D<sup>+</sup> and H<sub>2</sub>, the H<sub>2</sub>D<sup>+</sup> OPR is given as a function of the H<sub>2</sub> OPR and gas temperature

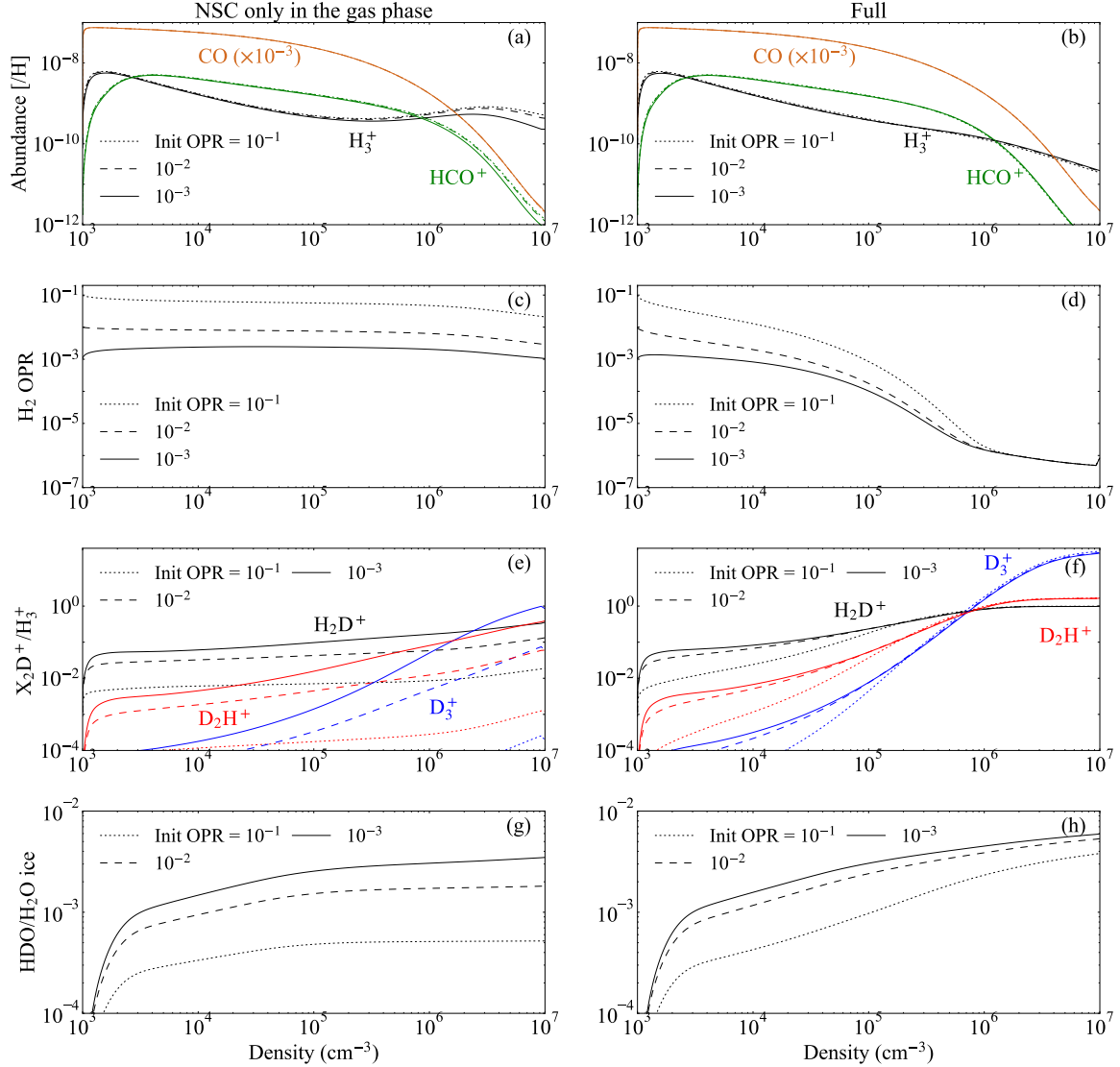


**Figure 7.** The evolution of the abundances and abundance ratios in the collapse model with (right panels) and without (left panels) the NSC on grains. Solid, dashed, and dotted lines represent models with the initial  $H_2$  OPR of  $10^{-3}$ ,  $10^{-2}$ , and  $10^{-1}$ , respectively. (a), (b) the abundances of selected species. (c), (d) the  $H_2$  OPR. (e), (f) the  $X_2D^+/H_3^+$  abundance ratio, where  $X$  represents H or D. (g), (h) the icy HDO/H<sub>2</sub>O ratio. In panels (a) and (b), the CO abundance is multiplied by  $10^{-3}$  to increase the visibility, the  $H_3^+$  abundance is the sum of ortho and para states, and the models with the different initial  $H_2$  OPR are depicted with the same color, because it does not significantly affect the abundances of the selected species. As the density increases with time on the free-fall timescale in the model, the horizontal axes can be read as time.

(Gerlich et al. 2002; Brünken et al. 2014). Then, if the gas temperature is given, the OPR of H<sub>2</sub> and that of H<sub>2</sub>D<sup>+</sup> have a one-to-one relation. Brünken et al. (2014) detected o-H<sub>2</sub>D<sup>+</sup> and p-H<sub>2</sub>D<sup>+</sup> in the cold outer envelope of the Class 0 protostellar source IRAS 16293-2422. They derived the H<sub>2</sub>D<sup>+</sup> OPR of  $0.065 \pm 0.019$  in the region with the gas temperature of 13-16 K, which corresponds to the H<sub>2</sub> OPR of  $\sim 2 \times 10^{-4}$ . In order to interpret the low H<sub>2</sub> OPR, they performed pseudo-time-dependent astrochemical simulations with the physical conditions appropriate for the cold outer envelope, assuming the initial H<sub>2</sub> OPR of  $10^{-3}$ . They claimed that to reduce the H<sub>2</sub>D OPR and H<sub>2</sub> OPR to the level derived from the observations, it takes more than 1 Myr, which is longer than the typical lifetime of the Class 0 stage (Dunham et al. 2014). Because their astrochemical model did not consider the NSC of H<sub>2</sub> on grain surfaces, their estimated timescale should be regarded as the upper limit value. It should be noted that the estimated timescale by Brünken et al. (2014) has been questioned; Harju et al. (2017) re-estimated the timescale of 0.5 Myr by using a pseudo-time-dependent astrochemical model similar to that of Brünken et al. (2014), but considered both the H<sub>2</sub>D<sup>+</sup>

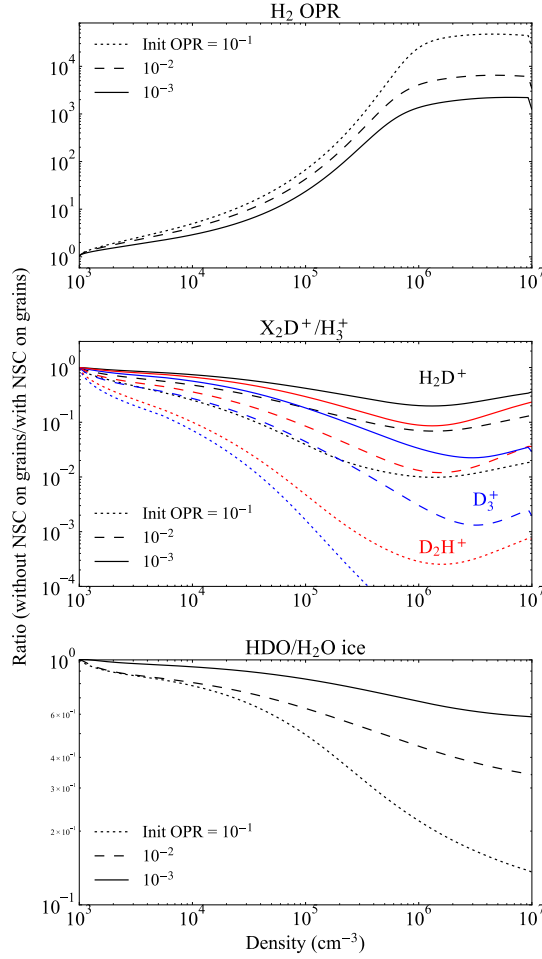


**Figure 8.** Ratio of the results obtained without and with NSC on grains in the collapse model: (top) H<sub>2</sub> OPR, (middle) X<sub>2</sub>D<sup>+</sup>/H<sub>3</sub><sup>+</sup>, where X is H or D, and (bottom) icy HDO/H<sub>2</sub>O. Solid, dashed, and dotted lines represent models with the initial H<sub>2</sub> OPR of 10<sup>-3</sup>, 10<sup>-2</sup>, and 10<sup>-1</sup>, respectively.

and D<sub>2</sub>H<sup>+</sup> data toward IRAS 16293-2422 in their analysis. Bovino et al. (2021), on the other hand, proposed even shorter timescale, 0.2 Myr, employing three-dimensional magneto-hydrodynamical simulations of collapsing filaments to form cores, coupled with chemistry, rather than pseudo-time-dependent astrochemical models. Neither of these studies considered NSC on grains. The main purpose of this section is not to estimate the most accurate timescale, but to demonstrate that even with a simple model setup similar to Brünken et al. (2014), the inclusion of NSC on grains can alter the conclusion.

To check the impact of the NSC on grains on the estimated timescale, we run our astrochemical models described in Section 4 with a similar setting to the model of Brünken et al. (2014), but considering the NSC on grains. We consider three cases with different  $\Delta E_{\text{op,s}}$ ; 170.5 K, 120 K, and 85 K. In all simulations, the gas density is set to 10<sup>5</sup> cm<sup>-3</sup> and  $A_V$  is set to 10 mag. Gas and dust temperatures are assumed to be the same and vary between 10 K to 20 K. The initial H<sub>2</sub> OPR is set to 10<sup>-3</sup> as in Brünken et al. (2014). The upper panels of Figure 9 shows the H<sub>2</sub>D<sup>+</sup> OPR as a function of the temperature at different times. The simulation results with  $\Delta E_{\text{op,s}} = 85$  K are not shown in Fig. 9, as they are essentially similar to those with  $\Delta E_{\text{op,s}} = 120$  K. As found in Brünken et al. (2014), when only the NSC in the gas-phase is considered, it takes  $\sim 1$  Myr to reach the observed level of the H<sub>2</sub>D<sup>+</sup> OPR. On the other hand, when the NSC on grains is additionally considered, 0.1 Myr is long enough to explain the observed H<sub>2</sub>D<sup>+</sup> OPR at the temperature of 12 K - 16 K. Exceptionally, when  $\Delta E_{\text{op,s}} = 170.5$  K and  $T = 16$  K, NSC on grains is less efficient than the NSC in the gas-phase, and still 1 Myr timescale is required. The simulation results with  $\Delta E_{\text{op,s}} = 85$  K are not shown in Fig. 9, as they are essentially similar to those with  $\Delta E_{\text{op,s}} = 120$  K. The above results hold even when we assume the initial H<sub>2</sub> OPR of 10<sup>-2</sup> as shown in the lower panels of the figure.

A caveat for the above discussion is that our model used the experimentally derived binding energy distribution of H<sub>2</sub> and the NSC rate on water ice surfaces. In star- and planet-forming regions, gaseous H<sub>2</sub> would interact with not only water ice surfaces, but also various types of surfaces, including CO, CO<sub>2</sub>, and CH<sub>3</sub>OH ices. To the best of our knowledge, similar experimental measurements that are adequate for ices other than water are not available in the literature. Once such measurements become available, it is straightforward to run similar simulations to those done here. On the other hand, Kouchi et al. (2021) has proposed that in molecular clouds, CO<sub>2</sub> nano-crystals are embedded in the amorphous H<sub>2</sub>O ice, and a polyhedral CO crystal is attached to the amorphous H<sub>2</sub>O. If this is the case, most H<sub>2</sub> could interact with amorphous H<sub>2</sub>O ice even if other species than water exist on grain surfaces.

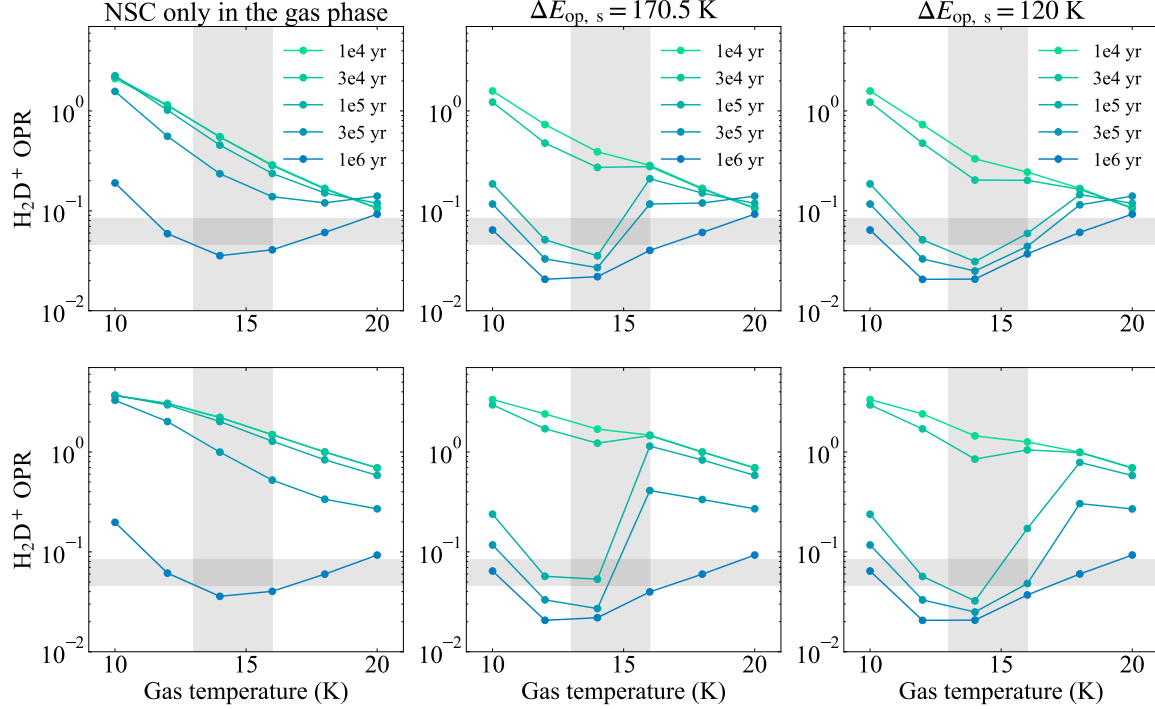


**Figure 9.** Temporal evolution of the H<sub>2</sub>D<sup>+</sup> OPR predicted in the model without (left) and with the NSC on grains assuming  $\Delta E_{\text{op},s} = 170.5$  K (middle) or 120 K (right). The gas density is set to  $10^5 \text{ cm}^{-3}$ , while the temperature varies from 10 K to 20 K. The gray areas indicate the H<sub>2</sub>D<sup>+</sup> OPR and the gas temperature constrained by the observations toward IRAS 16293-2422 (Brünken et al. 2014). The upper and lower panels correspond to the cases when the initial H<sub>2</sub> OPR is  $10^{-3}$  and  $10^{-2}$ , respectively.

### 5.2. Conditions under which NSC on grains and $\Delta E_{\text{op},s}$ are important

As shown above, the NSC on grains is more efficient than that in the gas phase at densities of  $\gtrsim 10^4 \text{ cm}^{-3}$  and temperatures of  $\lesssim 14\text{-}16$  K, depending on  $\Delta E_{\text{op},s}$ . The evolution of the H<sub>2</sub> OPR in lower density regions ( $\lesssim 10^4 \text{ cm}^{-3}$ ) was studied by Furuya et al. (2015), using a simple 1D model of the molecular cloud formation driven by shock compression of atomic gas, and gas-ice chemical network calculations in post-processing. They found that during the transition from atomic to molecular hydrogen, the NSC in the gas phase is efficient ( $\tau_{\text{op},g} < \tau_{\text{H}_2}$ ) and that the H<sub>2</sub> OPR becomes lower than the statistical value of three ( $\lesssim 0.1$ ) before the conversion of atomic H into H<sub>2</sub> is nearly complete (see their Appendix C for details). Lupi et al. (2021) performed 3D hydrodynamical simulations of collapsing filaments coupled with chemistry and found that the H<sub>2</sub> OPR decrease to  $\sim 10^{-3}\text{-}10^{-2}$  due to the NSC in the gas phase before the gas density reaches  $\sim 10^4 \text{ cm}^{-3}$ .

It should be noted that the evolution of the H<sub>2</sub> OPR via the NSC in the gas phase may be affected by the elemental abundance of gas-phase sulfur (Furuya et al. 2015). A higher sulfur abundance reduce the efficiency of the NSC in the gas phase, because H<sup>+</sup>, which is the key species for the NSC, is destroyed by abundant S atoms and CS. In a specific model of Furuya et al. (2015), if the non-depleted (i.e., solar) sulfur elemental abundance is adopted, the H<sub>2</sub> OPR remains high ( $> 10^{-2}$ ) at the end of their simulations ( $\sim 10$  Myr after the shock compression), whereas adopting a low

sulfur elemental abundance (depletion factor of  $\sim 100$ ) yields an the H<sub>2</sub> OPR as low as  $10^{-3}$ . The chemical network of Lupi et al. (2021) did not include any sulfur-bearing species. Recent molecular line observations toward molecular clouds indicate that the level of gas-phase sulfur depletion is smaller than previously thought and vary among clouds from a factor of  $\sim 20$  (Taurus and Perseus molecular clouds) to no depletion (Orion) (Fuente et al. 2023). It would be important to simulate the H<sub>2</sub> OPR evolution together with sulfur chemistry using 3D hydrodynamical simulations for better quantifying the H<sub>2</sub> OPR in relatively low density regions of  $\lesssim 10^4 \text{ cm}^{-3}$ .

When the H<sub>2</sub> OPR is  $\sim 10^{-3}$ , the destruction rate of H<sub>2</sub>D<sup>+</sup> by H<sub>2</sub> is comparable to that by CO, assuming a CO abundance of  $\sim 10^{-4}$  relative to H<sub>2</sub> (Furuya et al. 2015). Thus, even if a relatively low H<sub>2</sub> OPR ( $\sim 10^{-2}$  or lower) is established during the formation and evolution of molecular clouds with densities lower than  $\sim 10^4 \text{ cm}^{-3}$ , it would still not low enough for extreme deuterium fractionation observed in denser, prestellar cores: the very high D/H ratio of  $> 0.1$  for e.g., N<sub>2</sub>H<sup>+</sup> (Crapsi et al. 2005) and CH<sub>3</sub>OH (Spezzano et al. 2025) and abundant doubly deuterated species (Chacón-Tanarro et al. 2019). Further reduction of the H<sub>2</sub> OPR would be required and it would be driven mainly by the NSC on grains (see Section 4). An accurate treatment of grain-surface NSC is therefore important for modeling deuterium chemistry in prestellar cores and other dense regions, such as protoplanetary disks (Aikawa et al. 2018).

On the other hand, in the central regions of prestellar cores without nearby star formation activity, dust temperatures are expected to be below 10 K (e.g., Keto & Caselli 2010; Hocuk et al. 2017). At such low temperatures, the exact value of  $\Delta E_{\text{op},s}$  is not important for the efficiency of the NSC. The  $\Delta E_{\text{op},s}$  value becomes important only in slightly warmer regions ( $\sim 15$  K), such as the outer envelopes of low-mass protostars (as discussed in Section 5), prestellar cores exposed to strong external radiation fields (e.g., from nearby stars), or the midplane of the outer regions of protoplanetary disks.

## 6. SUMMARY

We have investigated how the H<sub>2</sub> OPR and deuterium fractionation in star-forming regions is affected by the NSC on dust grains, focusing on the rotational energy difference between o-H<sub>2</sub> and p-H<sub>2</sub> on grain surfaces ( $\Delta E_{\text{op},s}$ ). The previous work by Furuya et al. (2019) developed a rigorous formulation for the conversion rate of gas-phase o-H<sub>2</sub> (p-H<sub>2</sub>) to gas-phase p-H<sub>2</sub> (o-H<sub>2</sub>) via the NSC on grains, assuming that adsorbed o-H<sub>2</sub> has higher rotational energy than adsorbed p-H<sub>2</sub> by 170.5 K, as in the gas phase. However, their energy difference can be lower than 170.5 K, because interactions between the surface and adsorbed H<sub>2</sub> molecules affect their rotational motion. In this work, we relax the assumption in Furuya et al. (2019) and re-evaluate the conversion rate between o-H<sub>2</sub> and p-H<sub>2</sub>. We have found that the conversion rate depends on  $\Delta E_{\text{op},s}$ . On the other hand the steady-state H<sub>2</sub> OPR determined solely by the NSC on grains is largely insensitive to  $\Delta E_{\text{op},s}$ , because two effects ( $\Delta E_{\text{op},s} \leq \Delta E_{\text{op},g}$  and higher binding energy of o-H<sub>2</sub> than p-H<sub>2</sub>) are canceled out, even when various different binding sites and thermal hopping among them are considered. Therefore, regardless of  $\Delta E_{\text{op},s}$ , one can include the NSC on grains in any astrochemical kinetic models with the slightly modified version of the formulation by Furuya et al. (2019) (Eqs. 6, 7, and 17). When the dust temperature is  $\lesssim 14\text{--}16$  K (depending on  $\Delta E_{\text{op},s}$ ), and the gas density is higher than  $10^4 \text{ cm}^{-3}$ , the NSC on grains can be more important than that via the gas-phase proton-exchange reactions (see Sections 3 and 5.2 for details).

Finally, we have added the NSC on grain surfaces to the existing gas-ice astrochemical model with deuterated species and the nuclear spin states of light species. As case studies, we have investigated the time evolution of the H<sub>2</sub> OPR and deuterium fractionation in collapsing prestellar cores and in the outer envelope of the low mass protostar. In the prestellar core model, the deuterium fractionation is more efficient at  $\gtrsim 10^5 \text{ cm}^{-3}$  in the case when the NSC on grains compared to the case without the NSC on grains (the D/H ratio for H<sub>3</sub><sup>+</sup> isotopologues can be enhanced by a factor of 10 or more). In addition, the dependence of the D/H ratio for H<sub>3</sub><sup>+</sup> isotopologues on the initial H<sub>2</sub> OPR becomes weaker by considering the NSC on grains. In the protostellar envelope model, we have found that by considering NSC on grains, 10<sup>5</sup> yr is long enough for the H<sub>2</sub>D<sup>+</sup> OPR to reach the observed value by Brünken et al. (2014), while when only NSC in the gas phase is considered,  $\sim 10^6$  yr is required to explain the observed level of the H<sub>2</sub>D<sup>+</sup> OPR as claimed by Brünken et al. (2014).

## ACKNOWLEDGMENTS

We would like to thank the anonymous referees for their useful comments. This work is supported in part by JSPS KAKENHI Grant numbers 20H05847, 22H00296, 24K00686, and 25K07364.

Software: Matplotlib (Hunter 2007)

## APPENDIX

### A. ENERGY DIFFERENCE BETWEEN ADSORBED ORTHO AND PARA HYDROGEN

The surface potential  $V(z, \theta)$  of a molecule is mainly characterized by its well-depth and anisotropy as functions of the distance ( $z$ ) between the mass center of the molecule and the surface, and the molecular-axis angle ( $\theta$ ) with respect to the surface normal. When the degree of anisotropy is not so large, the surface potential is simply approximated as  $V(z, \theta) = V_0(z) + V_2 P_2(\cos \theta)$ , where  $P_2(\cos \theta)$  is the second order Legendre polynomial, and  $V_0(z)$  and  $V_2$  are the isotropic surface potential and the degree of anisotropy, respectively (Yu et al. 1985; Whaley et al. 1985). Moreover, when the anisotropic surface field is not so large, the  $V_2 P_2(\cos \theta)$  term can be treated as the first-order perturbation relative to the free molecular rotation in the isotropic  $V_0(z)$  potential. Within the first-order perturbation, the wave function is regarded unaltered, whereas the rotational energy shift is represented as follows (Andersson & Harris 1982; Nordlander et al. 1985):

$$\begin{aligned}\Delta E_{\text{shift}}(J, m) &= V_2 \langle J, m | P_2(\cos \theta) | J, m \rangle \\ &= \frac{3}{2J+3} \left( \frac{J^2 - m^2}{2J-1} - \frac{J}{3} \right) V_2,\end{aligned}\quad (\text{A1})$$

where  $|J, m\rangle$  is the rotational wave function written by spherical harmonics  $Y_{J,m}(\theta, \phi)$  and  $m$  is the  $z$  component of  $J$ . The rotational matrix element is given in Andersson & Harris (1982); Nordlander et al. (1985); Fukutani & Sugimoto (2013). Whereas the  $J = 0$  state (p-H<sub>2</sub>) shows no shift, the  $m$  degeneracy of  $J = 1$  state (o-H<sub>2</sub>) is lifted with an energy splitting of  $3V_2/5$ ; the  $(J, m) = (1, 0)$  and  $(1, \pm 1)$  rotational states are shifted by  $\Delta E_{\text{shift}}(1, 0) = 2V_2/5$  and  $\Delta E_{\text{shift}}(1, \pm 1) = -V_2/5$ , respectively (Figure 2). When  $V_2$  is negative, the ground state of o-H<sub>2</sub> is  $(J, m) = (1, 0)$  (i.e., no rotational degeneracy), and the energy difference between the ground states of p-H<sub>2</sub> and o-H<sub>2</sub> is  $\Delta E_{\text{op},s} = \Delta E_{\text{op},g} + \Delta E_{\text{shift}}(1, 0) = 2B + 2V_2/5$  (Figure 2). In contrast, when  $V_2$  is positive, the ground state of o-H<sub>2</sub> is  $(J, m) = (1, \pm 1)$  (the rotational degeneracy is 2), and the energy difference between the ground states of p-H<sub>2</sub> and o-H<sub>2</sub> is  $\Delta E_{\text{op},s} = 2B - V_2/5$  (Figure 2). Depending on the sign of  $V_2$ , the rotational motion tends to be restricted to either the surface-normal direction (1D hindered rotation) for negative  $V_2$ , or the surface-parallel direction (2D hindered rotation) for positive  $V_2$ .

In the case of metal surfaces, e.g., Ag(111) and Au(110),  $V_2$  is around -5 meV (Sugimoto & Fukutani 2014; Sugimoto et al. 2017). Then the rotational energy difference between the lowest rotational level of p-H<sub>2</sub> and o-H<sub>2</sub> is estimated to be  $\Delta E_{\text{op},s} \sim 12.8$  meV ( $\sim 150$  K) that is larger than  $\Delta E_{\text{op},2\text{Drot}} \sim 7.4$  meV ( $\sim 85$  K) but smaller than  $\Delta E_{\text{op},g} \sim 14.8$  meV ( $\sim 170$  K). As ASW is more highly anisotropic than metals,  $\Delta E_{\text{op},s}$  on ASW would be somewhere between that on the metals and  $\Delta E_{\text{op},2\text{Drot}}$ .

## REFERENCES

Aikawa, Y., Furuya, K., Hincelin, U., & Herbst, E. 2018, ApJ, 855, 119, doi: [10.3847/1538-4357/aaad6c](https://doi.org/10.3847/1538-4357/aaad6c)

Aikawa, Y., Furuya, K., Nomura, H., & Qi, C. 2015, ApJ, 807, 120, doi: [10.1088/0004-637X/807/2/120](https://doi.org/10.1088/0004-637X/807/2/120)

Aikawa, Y., & Herbst, E. 1999, ApJ, 526, 314, doi: [10.1086/307973](https://doi.org/10.1086/307973)

Amiaud, L., Fillion, J.-H., Dulieu, F., Momeni, A., & Lemaire, J.-L. 2015, Physical Chemistry Chemical Physics (Incorporating Faraday Transactions), 17, 30148, doi: [10.1039/C5CP03985A](https://doi.org/10.1039/C5CP03985A)

Andersson, S., & Harris, J. 1982, Phys. Rev. Lett., 48, 545, doi: [10.1103/PhysRevLett.48.545](https://doi.org/10.1103/PhysRevLett.48.545)

Bovino, S., Grassi, T., Schleicher, D. R. G., & Caselli, P. 2017, ApJL, 849, L25, doi: [10.3847/2041-8213/aa95b7](https://doi.org/10.3847/2041-8213/aa95b7)

Bovino, S., Lupi, A., Giannetti, A., et al. 2021, A&A, 654, A34, doi: [10.1051/0004-6361/202141252](https://doi.org/10.1051/0004-6361/202141252)

Bron, E., Le Petit, F., & Le Bourlot, J. 2016, A&A, 588, A27, doi: [10.1051/0004-6361/201527879](https://doi.org/10.1051/0004-6361/201527879)

Brown, P. D., & Millar, T. J. 1989, Monthly Notices of the Royal Astronomical Society, 237, 661, doi: [10.1093/mnras/237.3.661](https://doi.org/10.1093/mnras/237.3.661)

Brünken, S., Sipilä, O., Chambers, E. T., et al. 2014, Nature, 516, 219, doi: [10.1038/nature13924](https://doi.org/10.1038/nature13924)

Cazaux, S., Martín-Doménech, R., Chen, Y. J., Muñoz Caro, G. M., & González Díaz, C. 2017, ApJ, 849, 80, doi: [10.3847/1538-4357/aa8b0c](https://doi.org/10.3847/1538-4357/aa8b0c)

Cecarelli, C., Caselli, P., Bockelée-Morvan, D., et al. 2014, in Protostars and Planets VI, ed. H. Beuther, R. S. Klessen, C. P. Dullemond, & T. Henning, 859, doi: [10.2458/azu-uapress\\_9780816531240-ch037](https://doi.org/10.2458/azu-uapress_9780816531240-ch037)

Chacón-Tanarro, A., Caselli, P., Bizzocchi, L., et al. 2019, A&A, 622, A141, doi: [10.1051/0004-6361/201832703](https://doi.org/10.1051/0004-6361/201832703)

Cooper, A. M., & Kästner, J. 2019, Journal of Physical Chemistry A, 123, 9061, doi: [10.1021/acs.jpca.9b07013](https://doi.org/10.1021/acs.jpca.9b07013)

Crapsi, A., Caselli, P., Walmsley, C. M., et al. 2005, ApJ, 619, 379, doi: [10.1086/426472](https://doi.org/10.1086/426472)

Dunham, M. M., Stutz, A. M., Allen, L. E., et al. 2014, in Protostars and Planets VI, ed. H. Beuther, R. S. Klessen, C. P. Dullemond, & T. Henning, 195–218, doi: [10.2458/azu-uapress\\_9780816531240-ch009](https://doi.org/10.2458/azu-uapress_9780816531240-ch009)

Flower, D. R., Pineau Des Forêts, G., & Walmsley, C. M. 2006, A&A, 449, 621, doi: [10.1051/0004-6361:20054246](https://doi.org/10.1051/0004-6361:20054246)

Fuente, A., Rivièvre-Marichalar, P., Beitia-Antero, L., et al. 2023, A&A, 670, A114, doi: [10.1051/0004-6361/202244843](https://doi.org/10.1051/0004-6361/202244843)

Fukutani, K., & Sugimoto, T. 2013, Progress In Surface Science, 88, 279, doi: [10.1016/j.progsurf.2013.09.001](https://doi.org/10.1016/j.progsurf.2013.09.001)

Furuya, K. 2024, ApJ, 974, 115, doi: [10.3847/1538-4357/ad6b20](https://doi.org/10.3847/1538-4357/ad6b20)

Furuya, K., Aikawa, Y., Hama, T., & Watanabe, N. 2019, ApJ, 882, 172, doi: [10.3847/1538-4357/ab3790](https://doi.org/10.3847/1538-4357/ab3790)

Furuya, K., Aikawa, Y., Hincelin, U., et al. 2015, A&A, 584, A124, doi: [10.1051/0004-6361/201527050](https://doi.org/10.1051/0004-6361/201527050)

Furuya, K., Hama, T., Oba, Y., et al. 2022, ApJL, 933, L16, doi: [10.3847/2041-8213/ac78e9](https://doi.org/10.3847/2041-8213/ac78e9)

Garrod, R. T., & Pauly, T. 2011, ApJ, 735, 15, doi: [10.1088/0004-637X/735/1/15](https://doi.org/10.1088/0004-637X/735/1/15)

Gerlich, D. 1990, JChPh, 92, 2377, doi: [10.1063/1.457980](https://doi.org/10.1063/1.457980)

Gerlich, D., Herbst, E., & Roueff, E. 2002, Planet. Space Sci., 50, 1275, doi: [10.1016/S0032-0633\(02\)00094-6](https://doi.org/10.1016/S0032-0633(02)00094-6)

Goldsmith, P. F., & Li, D. 2005, ApJ, 622, 938, doi: [10.1086/428032](https://doi.org/10.1086/428032)

Harju, J., Sipilä, O., Brünken, S., et al. 2017, ApJ, 840, 63, doi: [10.3847/1538-4357/aa6c69](https://doi.org/10.3847/1538-4357/aa6c69)

Hasegawa, T. I., & Herbst, E. 1993, MNRAS, 263, 589, doi: [10.1093/mnras/263.3.589](https://doi.org/10.1093/mnras/263.3.589)

He, J., Acharyya, K., & Vidali, G. 2016, ApJ, 823, 56, doi: [10.3847/0004-637X/823/1/56](https://doi.org/10.3847/0004-637X/823/1/56)

He, J., & Vidali, G. 2014, Faraday Discussions, 168, 517, doi: [10.1039/C3FD00113J](https://doi.org/10.1039/C3FD00113J)

Hidaka, H., Watanabe, M., Kouchi, A., & Watanabe, N. 2009, ApJ, 702, 291, doi: [10.1088/0004-637X/702/1/291](https://doi.org/10.1088/0004-637X/702/1/291)

Hillenbrand, P. M., Bowen, K. P., Liévin, J., Urbain, X., & Savin, D. W. 2019, ApJ, 877, 38, doi: [10.3847/1538-4357/ab16dc](https://doi.org/10.3847/1538-4357/ab16dc)

Hily-Blant, P., Faure, A., Rist, C., Pineau des Forêts, G., & Flower, D. R. 2018, MNRAS, 477, 4454, doi: [10.1093/mnras/sty881](https://doi.org/10.1093/mnras/sty881)

Hocuk, S., Szűcs, L., Caselli, P., et al. 2017, A&A, 604, A58, doi: [10.1051/0004-6361/201629944](https://doi.org/10.1051/0004-6361/201629944)

Honvault, P., Jorfi, M., González-Lezana, T., Faure, A., & Pagani, L. 2011, PhRvL, 107, 023201, doi: [10.1103/PhysRevLett.107.023201](https://doi.org/10.1103/PhysRevLett.107.023201)

—. 2012, PhRvL, 108, 109903, doi: [10.1103/PhysRevLett.108.109903](https://doi.org/10.1103/PhysRevLett.108.109903)

Hugo, E., Asvany, O., & Schlemmer, S. 2009, JChPh, 130, 164302, doi: [10.1063/1.3089422](https://doi.org/10.1063/1.3089422)

Hunter, J. D. 2007, Computing in Science & Engineering, 9, 90, doi: [10.1109/MCSE.2007.55](https://doi.org/10.1109/MCSE.2007.55)

Jiménez-Redondo, M., Sipilä, O., Jusko, P., & Caselli, P. 2024, A&A, 692, A121, doi: [10.1051/0004-6361/202451757](https://doi.org/10.1051/0004-6361/202451757)

Keto, E., & Caselli, P. 2010, MNRAS, 402, 1625, doi: [10.1111/j.1365-2966.2009.16033.x](https://doi.org/10.1111/j.1365-2966.2009.16033.x)

Kouchi, A., Tsuge, M., Hama, T., et al. 2021, ApJ, 918, 45, doi: [10.3847/1538-4357/ac0ae6](https://doi.org/10.3847/1538-4357/ac0ae6)

Le Bourlot, J. 1991, A&A, 242, 235

Le Petit, F., Ruaud, M., Bron, E., et al. 2016, A&A, 585, A105, doi: [10.1051/0004-6361/201526658](https://doi.org/10.1051/0004-6361/201526658)

Linsky, J. L. 2003, SSRv, 106, 49, doi: [10.1023/A:1024673217736](https://doi.org/10.1023/A:1024673217736)

Lupi, A., Bovino, S., & Grassi, T. 2021, A&A, 654, L6, doi: [10.1051/0004-6361/202142145](https://doi.org/10.1051/0004-6361/202142145)

Maret, S., & Bergin, E. A. 2007, ApJ, 664, 956, doi: [10.1086/519152](https://doi.org/10.1086/519152)

Millar, T. J., Bennett, A., & Herbst, E. 1989, ApJ, 340, 906, doi: [10.1086/167444](https://doi.org/10.1086/167444)

Molpeceres, G., & Kästner, J. 2020, Physical Chemistry Chemical Physics (Incorporating Faraday Transactions), 22, 7552, doi: [10.1039/D0CP00250J](https://doi.org/10.1039/D0CP00250J)

Nagaoka, A., Watanabe, N., & Kouchi, A. 2005, ApJL, 624, L29, doi: [10.1086/430304](https://doi.org/10.1086/430304)

Nomura, H., Furuya, K., Cordiner, M. A., et al. 2023, in Astronomical Society of the Pacific Conference Series, Vol. 534, Protostars and Planets VII, ed. S. Inutsuka, Y. Aikawa, T. Muto, K. Tomida, & M. Tamura, 1075

Nordlander, P., Holmberg, C., & Harris, J. 1985, Surface Science, 152-153, 702, doi: [https://doi.org/10.1016/0039-6028\(85\)90478-9](https://doi.org/10.1016/0039-6028(85)90478-9)

Pagani, L., Lesaffre, P., Jorfi, M., et al. 2013, A&A, 551, A38, doi: [10.1051/0004-6361/201117161](https://doi.org/10.1051/0004-6361/201117161)

Pagani, L., Roueff, E., & Lesaffre, P. 2011, *ApJL*, 739, L35, doi: [10.1088/2041-8205/739/2/L35](https://doi.org/10.1088/2041-8205/739/2/L35)

Pagani, L., Salez, M., & Wannier, P. G. 1992, *A&A*, 258, 479

Pagani, L., Vastel, C., Hugo, E., et al. 2009, *A&A*, 494, 623, doi: [10.1051/0004-6361:200810587](https://doi.org/10.1051/0004-6361:200810587)

Ratajczak, A., Quirico, E., Faure, A., Schmitt, B., & Ceccarelli, C. 2009, *A&A*, 496, L21, doi: [10.1051/0004-6361/200911679](https://doi.org/10.1051/0004-6361/200911679)

Roueff, E., Gerin, M., Lis, D. C., et al. 2013, *Journal of Physical Chemistry A*, 117, 9959, doi: [10.1021/jp400119a](https://doi.org/10.1021/jp400119a)

Sipilä, O., Caselli, P., & Harju, J. 2013, *A&A*, 554, A92, doi: [10.1051/0004-6361/201220922](https://doi.org/10.1051/0004-6361/201220922)

Sipilä, O., Harju, J., & Caselli, P. 2017, *A&A*, 607, A26, doi: [10.1051/0004-6361/201731039](https://doi.org/10.1051/0004-6361/201731039)

Spezzano, S., Riedel, W., Caselli, P., et al. 2025, arXiv e-prints, arXiv:2512.09110, doi: [10.48550/arXiv.2512.09110](https://doi.org/10.48550/arXiv.2512.09110)

Spitzer, L. 1978, Physical processes in the interstellar medium, doi: [10.1002/9783527617722](https://doi.org/10.1002/9783527617722)

Sugimoto, T., & Fukutani, K. 2014, *Phys. Rev. Lett.*, 112, 146101, doi: [10.1103/PhysRevLett.112.146101](https://doi.org/10.1103/PhysRevLett.112.146101)

Sugimoto, T., Kunisada, Y., & Fukutani, K. 2017, *Phys. Rev. B*, 96, 241409, doi: [10.1103/PhysRevB.96.241409](https://doi.org/10.1103/PhysRevB.96.241409)

Taquet, V., Charnley, S. B., & Sipilä, O. 2014, *ApJ*, 791, 1, doi: [10.1088/0004-637X/791/1/1](https://doi.org/10.1088/0004-637X/791/1/1)

Tielens, A. G. G. M. 1983, *A&A*, 119, 177

—. 2005, The Physics and Chemistry of the Interstellar Medium

Tsuge, M., Hama, T., Kimura, Y., Kouchi, A., & Watanabe, N. 2019, *ApJ*, 878, 23, doi: [10.3847/1538-4357/ab1e4e](https://doi.org/10.3847/1538-4357/ab1e4e)

Tsuge, M., Kouchi, A., & Watanabe, N. 2021a, *ApJ*, 923, 71, doi: [10.3847/1538-4357/ac2a33](https://doi.org/10.3847/1538-4357/ac2a33)

Tsuge, M., Namiyoshi, T., Furuya, K., et al. 2021b, *ApJ*, 908, 234, doi: [10.3847/1538-4357/abd9c0](https://doi.org/10.3847/1538-4357/abd9c0)

Ueta, H., Watanabe, N., Hama, T., & Kouchi, A. 2016, *PhRvL*, 116, 253201, doi: [10.1103/PhysRevLett.116.253201](https://doi.org/10.1103/PhysRevLett.116.253201)

Wakelam, V., Castets, A., Ceccarelli, C., et al. 2004, *A&A*, 413, 609, doi: [10.1051/0004-6361:20031572](https://doi.org/10.1051/0004-6361:20031572)

Watanabe, N., Kimura, Y., Kouchi, A., et al. 2010, *ApJL*, 714, L233, doi: [10.1088/2041-8205/714/2/L233](https://doi.org/10.1088/2041-8205/714/2/L233)

Watson, W. D. 1976, *Reviews of Modern Physics*, 48, 513, doi: [10.1103/RevModPhys.48.513](https://doi.org/10.1103/RevModPhys.48.513)

Whaley, K. B., Yu, C., Hogg, C. S., Light, J. C., & Sibener, S. J. 1985, *The Journal of Chemical Physics*, 83, 4235, doi: [10.1063/1.449087](https://doi.org/10.1063/1.449087)

Yu, C., Whaley, K. B., Hogg, C. S., & Sibener, S. J. 1985, *The Journal of Chemical Physics*, 83, 4217, doi: [10.1063/1.449086](https://doi.org/10.1063/1.449086)